FRICTION STIR PROCESSING OF ALUMINUM ALLOY 7075 REINFORCED WITH YTTRIUM OXIDE NANO POWDER

2024
MASTER THESIS
METALLURGICAL AND MATERIALS ENGINEERING

Ahmed Abdullah Khalaf KHALAF

Thesis Advisors
Assoc. Prof. Dr. Hüseyin DEMİRTAŞ
Assist. Prof. Dr. Ahmed Ameed ZAINULABDEEN

FRICTION STIR PROCESSING OF ALUMINUM ALLOY 7075 REINFORCED WITH YTTRIUM OXIDE NANO POWDER

Ahmed Abdullah Khalaf KHALAF

Thesis Advisors
Assoc. Prof. Dr. Hüseyin DEMİRTAŞ
Assist. Prof. Dr. Ahmed Ameed ZAINULABDEEN

T.C.
Karabuk University
Institute of Graduate Programs
Department of Metallurgical and Materials Engineering
Prepared as
Master Thesis

KARABUK
June 2024

I certify that in my opinion the thesis submitted by Ahmed Abdullah Khalaf titled "FRICTION STIR PROCESSING OF ALUMINUM ALLOY 7075 REINFORCED WITH YTTRIUM OXIDE NANO POWDER" is fully adequate in scope and in quality as a thesis for the degree of Master of Science.

Assoc. Prof. Dr. Hüseyin DEMİRTAŞ .....

Thesis Advisor, Department of Metallurgical and Materials Engineering.

Assist. Prof. Dr. Ahmed Ameed Zainulabdeen .....

Thesis Advisor, University of Technology – Baghdad, Iraq, Materials Engineering Department.

This thesis is accepted by the examining committee with a unanimous vote in the Department of Metallurgical and Materials Engineering as a Master of Science thesis. June 25, 2024

Examining Committee Members (Institutions)	Signature
Chairman: Prof. Dr. Fatih HAYAT (KBÜ)	.....
Member: Assist. Prof. Dr. Cihangir Tevfik SEZGİN (KÜ)	.....
Member: Assoc. Prof. Dr. Hüseyin DEMİRTAŞ (KBÜ)	.....

The degree of Master of Science by the thesis submitted is approved by the Administrative Board of the Institute of Graduate Programs, Karabuk University.

Assoc. Prof. Dr. Zeynep ÖZCAN .....

Director of the Institute of Graduate Programs

"I declare that all the information within this thesis has been gathered and presented in accordance with academic regulations and ethical principles and I have according to the requirements of these regulations and principles cited all those which do not originate in this work as well."

Ahmed Abdullah Khalaf KHALAF

ABSTRACT

M. Sc. Thesis

FRICTION STIR PROCESSING OF ALUMINUM ALLOY 7075 REINFORCED WITH YTTRIUM OXIDE NANO POWDER

Ahmed Abdullah Khalaf KHALAF

Karabuk University
Institute of Graduate Programs
Department of Metallurgical and Materials Engineering

Thesis Advisors:
Assoc. Prof. Dr. Hüseyin DEMİRTAŞ
Assist. Prof. Dr. Ahmed Ameed ZAINULABDEEN
June 2024, 77 pages

Friction stir processing (FSP) is a solid-state technique that leverages the principles of Friction stir welding (FSW) to refine microstructures and enhance mechanical properties. This method has gained significant attention in recent years for the fabrication of composites. It can produce multiphase composites by incorporating Yttrium Oxide (Y_2O_3) in powder form as secondary material during the FSP process. The incorporation of these secondary materials is achieved through various reinforcement strategies, which are crucial for ensuring proper mixing of the materials, controlled volume, and optimal physical and microstructural properties of the composites.

In this context, groove strategies are applied to achieve the desired reinforcement. The main aim of this study was to improve the mechanical properties of Al 7075-T73

using friction stir processing reinforcement with Y_2O_3 nano-powder with three rotational (710, 900 and 1120 rpm) and travel speeds (55, 70 and 90 mm/min) by using a cylindrical pin geometry with a tilt angle of 2 degrees.

In the process of 7075-T73 aluminum alloys, rotation speed 710 rpm and a travel speed 55 mm/min, and rotation speed 1120 rpm and a travel speed 55 mm/min were selected as optimum parameters in terms of wear rates.

Microhardness decreased with a travel speed of 55 mm/min and increased with 90 mm/min. The sample with a rotation speed of 1120 rpm and a travel speed of 90 mm/min was selected as the optimum parameters in terms of hardness value.

The highest yield strength value (407 MPa) obtained under processing conditions was associated with the specimen with rotation speed, travel speed and elongation percentage of 710 rpm, 55 mm/min and 1.4%, respectively.

Microstructural examinations show tunnels and accumulation of Y_2O_3 along the edge of the stir zone in some samples. SEM-EDS elemental analysis indicates good mixing in the stir zone and adequate diffusion of particles into Al 7075-T73. The stir zone produced finer grain compared to the base material.

Key Words: Aluminum alloys, Friction stir process, Tool rotation speed, Particle reinforced composites, Mechanical properties.

Science Code : 91512

ÖZET

Yüksek Lisans Tezi

NANO YİTRYUM OKSİT TOZU TAKVİYE EDİLMİŞ 7075 ALÜMİNYUM ALAŞIMININ SÜRTÜNME KARIŞTIRMA İŞLEMİ

Ahmed Abdullah Khalaf KHALAF

Karabük Üniversitesi
Lisansüstü Eğitim Enstitüsü
Metalürji ve Malzeme Mühendisliği Anabilim Dalı

Tez Danışmanları:
Doç. Dr. Hüseyin DEMİRTAŞ
Dr. Öğr. Üyesi Ahmed Ameed ZAINULABDEEN
Haziran 2024 77 sayfa

Sürtünme karıştırma işlemi (FSP), mikro yapıları iyileştirmek ve mekanik özellikleri geliştirmek için Sürtünme karıştırma kaynağı (FSW) ilkelerinden yararlanan bir katı hal işleme tekniğidir. Bu yöntem son yıllarda kompozitlerin üretiminde büyük ilgi görmüştür. FSP işlemi sırasında Yitrium Oksit'i (Y_2O_3) ikincil malzeme olarak toz halinde dahil ederek çok fazlı kompozitler üretebilir. Bu ikincil malzemelerin katılması, uygun şekilde karıştırılması ve kontrollü hacim kompozitlerin optimal fiziksel ve mikroyapısal özelliklerinin sağlanması için çok önemli olan çeşitli mukavemetlendirme stratejileriyle gerçekleştirilir.

Bu bağlamda istenilen takviyeyi elde etmek için oluk stratejileri uygulanır. Bu çalışmanın temel amacı, eğim açısı 2 derece olan silindirik bir pim geometrisi kullanılarak, üç dönme hızına (710, 900 ve 1120 rpm) ve ilerleme hızına (55, 70 ve

90 mm/dak) sahip sürtünme karıştırma işlemi ile Y_2O_3 nano toz takviyesi kullanarak Al 7075-T73'ün mekanik özelliklerini geliştirmektir.

7075-T73 alüminyum alaşımlarının prosesinde aşınma oranları yönünden dönme hızı 710 rpm ve ilerleme hızı 55 mm/dak ile dönme hızı 1120 rpm ve ilerleme hızı 55 mm/dak optimum parametreler olarak seçilmiştir.

Mikro sertlik 55 mm/dak ilerleme hızıyla azalırken, 90 mm/dak ilerleme hızıyla arttı. Dönme hızı 1120 rpm ve ilerleme hızı 90 mm/dak olan numune, sertlik değeri yönünden optimum numune olarak seçilmiştir.

İşleme koşulları altında elde edilen en yüksek akma mukavemeti değeri (407 MPa), sırasıyla dönme hızı, ilerleme hızı ve uzama yüzdesi 710 rpm, 55 mm/dak ve %1,4 olan numunede elde edilmiştir.

Mikroyapı incelemeleri bazı örneklerde karıştırma bölgesi kenarı boyunca tünelleri ve Y_2O_3'ün toplandığını göstermektedir. SEM-EDS element analizi, karıştırma bölgesinde iyi bir karışım olduğunu ve partiküllerin Al 7075-T73'e yeterli difüzyonunu gösterir. Karıştırma bölgesi, temel malzemeye kıyasla daha ince tanecik üretmiştir.

Anahtar Kelimeler: Alüminyum alaşımları, Sürtünme karıştırma işlemi, Takım dönüş hızı, Partikül takviyeli kompozitler, Mekanik özellikler

Bilim Kodu: 91512

ACKNOWLEDGMENT

First and before everyone I would like to thank God who helped me to complete this study. After that, I would like to thank my mother, wife and friends who supported me, and I would like to give thanks to my advisor, Assoc. Prof. Dr. Hüseyin DEMİRTAŞ and Assist. Prof. Dr. Ahmed Ameed ZAINULABDEEN for their great interest and assistance in the preparation of this thesis.

In addition, I would like to express of my thankfully to the MOE of Iraq Al-Musayyib Thermal Power Plant for supporting this study with using their workshop and milling machine, and the Department of Materials Engineering, University of Technology – Baghdad, Iraq for supporting this study by using their laboratories.

CONTENTS

Page

Page

Page

TABLE OF FIGURES

Page

Page

Page

TABLE OF TABLES

Page

SYMBOLS AND ABBREVITIONS INDEX

SYMBOLS

ISO	: International Organization for Standardization
ASTM	: American Society for Testing and Materials
Al	: Aluminum
Y_2O_3	: Yttrium Oxide
FSP	: Friction Stir Processing
FSW	: Friction Stir Welding
AFSP	: Additive Friction Stir Processing
SZ	: Stir Zone
HAZ	: Heat Affected Zone
TMAZ	: Thermomechanical Affected Zone
SCC	: Stress Corrosion Cracking
MMCs	: Metal Matrix Composites
OM	: Optical Microscope
XRD	: X-ray Diffraction
EDS	: Energy Dispersive Spectroscopy
SEM	: Scanning Electron Microscope

PART 1

INTRODUCTION

There is an increasing demand for reducing the weight of components in the automobile, Aircraft, and aerospace industries to enhance fuel efficiency. A new processing technique called friction stir processing (FSP) was developed by Mishra, and it is one of the severe plastic deformation techniques used for enhancing mechanical properties of materials by grain refinement. The FS technology consists of welding, processing, and additive processing. FSW is one of the most efficient solid states joining processes. It avoids many of the common problems of fusion welding. FSP is an effective solid state surface modification technique used to locally eliminate casting defects, refine microstructure, and improve the associated mechanical and physical properties including strength, ductility, fatigue, creep, formability, and corrosion resistance [1, 2].

There is basic three types of tools of FSW and FSP which are fixed, adjustable and self-reacting. The tool shoulders are basically designed to generate frictional heat in the surface regions of work piece and produce the downward forging action which is essential to constrain the heated metal under the bottom shoulder surface, and there are three types of shoulder end surfaces typically used, like flat, convex shoulder, and concave [3].

The FSW and FSP probes usually have a cylindrical outer surface and tapered outer shape, and the FSP has been composed of three different zones named stir zone SZ or nugget zone, thermomechanical affected zone (TMAZ) and heat affected zone HAZ. Additive friction stir processing (AFSP) can be used for coating, repair, manufacturing surface composites and additive manufacturing of similar or dissimilar materials [4].

1.1. FRICTION STIR PROCESSING

FSP is a solid-state processing technique that involves the use of a Rotational tool to generate frictional heat and plastic deformation in the material. The tool is inserted into the material and traversed along the processing direction, generating heat due to frictional forces between the tool and the material. The plastic deformation of the material caused by the tool results in a refined and homogenized microstructure [3]. FSP can be used to modify the microstructure and properties of various materials, including metals, alloys, and composites [5]. Figure 1.1 shows the classification of the FSP classification.

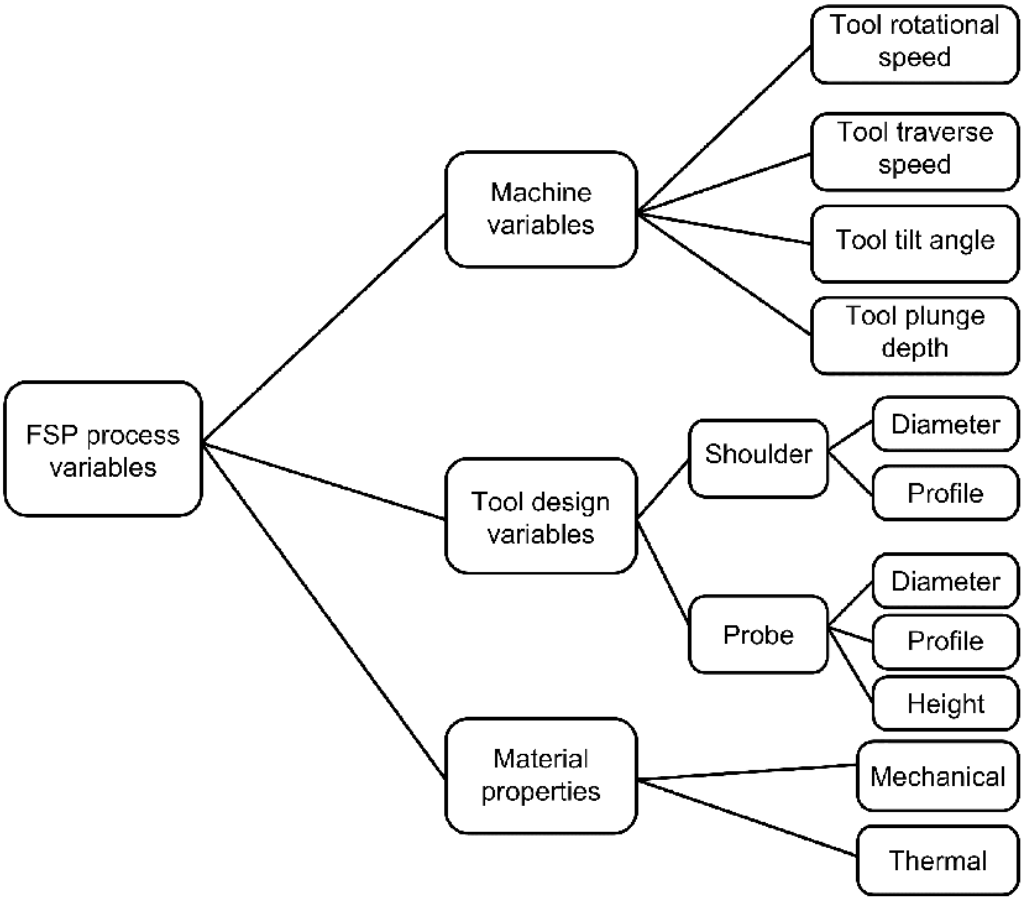

Figure 1.1. Schematic diagram of FSP process classification

1.2. ALUMINUM ALLOY / BRIEF OVERVIEW

An alloy in which Aluminum (Al) is the predominant metal, commonly alloyed with copper, magnesium, manganese, silicon, tin, nickel, and zinc, has a series from 1XXX to 8XXX shown in the Table 1.1. A comprehensive classification of Al alloys consists of two principal classifications: casting alloys and wrought alloys, further divided into heat-treatable and non-heat-treatable categories, widely used in engineering structures and components for its lightweight and corrosion resistance, with approximately 85% used for wrought products like rolled plate, foils, and extrusions. Crucial in aerospace manufacturing for creating metal-skinned aircraft, especially aluminum-magnesium alloys for their lighter weight and reduced flammability, Al surfaces can develop a protective layer of Al oxide if left unprotected by anodizing and/or correct painting procedures. Subject to galvanic corrosion in wet environments when in electrical contact with metals having more positive corrosion potentials, leading to exfoliation or intergranular corrosion, Al compositions are registered with the Al association and are subject to standards by organizations like the society of automotive engineers and ASTM International [6].

Table 1.1. A comprehensive classification of Al alloys

1.3. ALUMINUM ALLOY 7075

The Al 7075 was first developed in 1935 by Sumitomo Metal in Japan and was heavily employed in military aircraft production. It was reverse engineered in 1943 by Alcoa in US and was a significant component in the rapid improvement in military aircraft design among the allies [7].

Al 7075 alloy is known for its super high strength and was first used in the B-29 bomber, marking a significant milestone in the development of 7xxx series alloys. However, its use in aerospace was limited because of its low damage tolerance, poor corrosion resistance, and fracture toughness when used in thick large-section structures. To address these issues, researchers optimized heat treatment schedules, resulting in variants such as 7075-T73, T74, T76, and T651 and adjusted to enhance performance of the alloy composition. Reducing impurities like Si and Fe was found to improve fracture toughness, as these impurities lead to the formation of hard and thick intermetallic compounds that can initiate cracks, reducing the alloy's plasticity and toughness. The Al 7075-T73 is related to a successful double ageing process, which mitigates the stress corrosion problem of 7075-T6 alloy by sacrificing a small percentage of its strength. The T76 heat treatment was developed to enable the 7075 alloy to meet the requirements for stress corrosion cracking (SCC) and peeling corrosion resistance and only a slight reduction in strength. The chemical composition of 7075 and other 7xxx series alloys is detailed in Table 1.2. Aluminum alloys 7xxx series detailed of the document, showing the percentages of elements like Zn, Cu, Mg, Fe, Si, Mn, Ti, Cr and Zr, and the balance being aluminum. The document also discusses uses of Al alloys in aerospace various applications [8].

Table 1.2. Chemical composition (%) of 7xxx series Al alloys

7xxx series	Cu	Zn	Mg	Mn	Fe	Si	Cr	Zr	Ti	Al
7075	1.2~2.0	5.1~6.1	2.1~2.9	0.3	0.5	0.4	0.18~0.28	-	0.2	Bal.
7475	1.2~1.9	5.2~6.2	1.9~2.6	0.06	0.12	0.1	0.18~0.25	-	0.06	Bal.
7050	2.0~2.6	5.7~6.7	1.9~2.6	0.10	0.15	0.12	0.04	0.08~0.15	0.06	Bal.
7150	1.9~2.5	5.9~6.9	2.0~2.7	0.1	0.15	0.12	0.04	0.08~0.15	0.06	Bal.
7055	2.0~2.6	7.6~8.4	1.8~2.3	0.05	0.15	0.1	0.04	0.08~0.25	0.06	Bal.
7085	1.3~2.0	7.0~8.0	1.2~1.8	0.04	0.08	0.06	0.04	0.08~0.15	0.06	Bal.

1.4. PHYSICAL and MECHANICAL PROPERTIES of ALUMINUM ALLOYS 7075 and 7075– T73

Al 7075 has a higher percentage of Zn to this alloy makes 7075 one of the highest strength and hardest alloys available. Al 7075 has a melting point of around 475-635°C, depending on its specific composition and treatment and it has a density of approximately 2.81 g/cm^3.

This is heavier than some other aluminum alloys. It finds its most common where highly stressed parts are used in the aircraft industry. If annealed, this alloy is highly formable and may be flash or spot-welded. Heat-treating increases its strength considerably. In the "Alclad" condition, 7075 is highly resistant to corrosion [9, 10].

Al 7075-T73 is a very high strength material used for highly stressed structural parts, and it's improved the cracking resistance of stress-corrosion [11].

1.5. APPLICATIONS of Al 7075 – T73 Alloy

The search for effective and sustainable solutions has led researchers to focus on the applications of Al 7075-T73 alloy, which has significant implications for reducing various problems in various industries. One of the main areas of interest is the automotive sector, where the need for lightweight components is becoming

increasingly critical. The goal is to achieve lower fuel consumption and reduce leaks in vehicles, thus enhancing overall performance and reducing environmental impact.

The research in recent years work on development of alloys within the 7xxx series, including Al 7075-T73, has gained great attention. This increased focus is due to the need to meet the challenges posed by the automotive industry's demand for lightweight but durable components. Al alloy 7075-T73 has shown great promise in meeting these requirements because of its unique set of properties, including corrosion resistance, high strength-to-weight ratio and weldability [12].

The Al 7075-T73 uses fittings, upper and lower wings side, stringers, and frames for the aircrafts worm gears, fuse parts, meter shaft, missile parts, regulating valve parts, keys, aerospace, and defense applications [13, 14].

1.6. METAL MATRIX COMPOSITES

Metal matrix composites (MMCs) are composite materials consisting of a metallic matrix reinforced with one or more secondary phases, such as ceramic or metallic particles, fibers, or whiskers. MMCs exhibit high specific strength and stiffness, improved wear resistance, and good thermal and electrical conductivity, making them ideal for a wide range of applications [15].

MMCs reinforced with nanoparticles, and so-called Metal matrix nanocomposites (MMNCs), have promising properties for various applications. The main challenge in producing MMnCs is the low wettability of ceramic nanoparticles by molten metal, preventing the use of conventional casting methods. Several strengthening mechanisms contribute to MMnCs to the high mechanical resistance: Load transfer effect from the matrix to the stiff reinforcement particles under applied load. Hall-Petch strengthening: Grain refinement by nanoparticles pinning grain boundaries. Orowan strengthening: Interaction of nanoparticles with dislocations, causing dislocation bowing. Coefficient of thermal expansion (CTE) and elastic modulus (EM) mismatch: Formation of geometrically necessary dislocations because of CTE and EM differences between matrix and reinforcement. The most used matrix metals

are Al, Cu, Ti and Mg alloys. Ceramic reinforcements include oxides, nitrides, carbides, borides and carbon allotropes like CNTs. Powder metallurgy techniques like mechanical alloying and in-situ synthesis are widely used to produce MMnCs. These methods allow breaking up nano-particle clusters and achieving a homogeneous dispersion for optimal strengthening [16].

Aluminum metal matrix composites (AMMCs) are fabricated by incorporating desirable reinforcements. The addition of reinforcements leads to significant improvements in the mechanical and tribological properties of Al alloys, tensile strength, yield strength, compressive strength increases and hardness. With addition of MMCs reinforcement improves machinability and acts as a solid lubricant, reducing wear rate and coefficient of friction. Wear resistance increases with higher wt.% of reinforcements, Corrosion resistance improves, but can decrease overall with higher wt.% of reinforcements. AMMCs show superior properties compared to the base alloy and have wide applications [17].

1.7. YTTRIUM OXIDE

Yttrium oxide (Y_2O_3), also known as Yttria, is a white crystalline compound that is one of the most stable of the rare earth oxides. With a high melting point and a unique refractive index, yttria is commonly used as a stabilizing agent for zirconia in the production of various ceramic materials, particularly those used for high-temperature applications. Its excellent thermal stability and resistance to chemical attack make it valuable in the production of refractories, crucibles, and ceramic coatings exposed to high temperatures. Additionally, yttrium oxide is used in the manufacture of yttrium-iron garnets (YIGs), which have applications in microwave filters and resonators. The material also serves as a host lattice for phosphors in television tubes and white LEDs [18].

1.8. PROCESSING PARAMETERS for Al ALLOY REINFORCED with MMCS USING FSP

The processing parameters for FSP of AA reinforced by MMCs play a critical role in determining the microstructure and mechanical properties of the resulting composite. The key to parameters of processing included tool geometry, travel speed, rotational speed, axial force, MMCs particle size and volume fraction as shown in Figure 1.2. schematic diagram of reinforcement strategies [19].

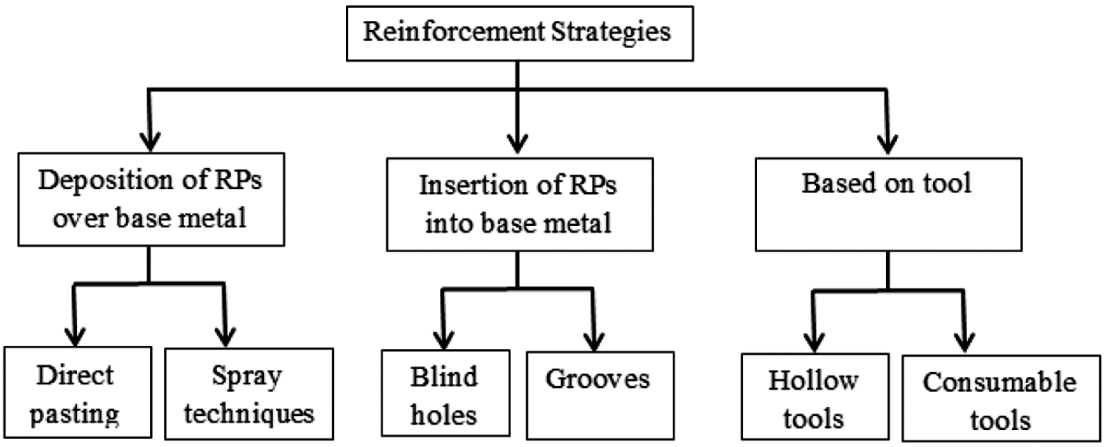

Figure 1.2. Schematic diagram of reinforcement strategies

1.8.1. Tool Material Selection

The FSW of aluminum alloys, the tool's wear is less. As such, tool materials such as tool steels can be used. However, in the FSP of high melting point materials that can wear out such as metal matrix composites (MMCs), tool wear has been noted to be a serious issue in such circumstances. It was also stated that tool material selection is important in FSP Metals and composites. Tool material selection may also be based on hardness, ductility, and reactivity of the work materials [20].

Several tool materials have been used in the FSW/P process. These materials include but are not limited to high-speed steel (HSS), tool steels, Ni-alloys, metal carbides and ceramics [21].

1.8.2. Tool Material Characteristics

To produce a high-quality FSP, it is a requirement that the tool material selection is done properly. The characteristics that have to be considered in choosing the tool material for FSW/P include resistance to wear, no harmful reactions to the weld metal, good strength, dimensional stability and creep resistance at ambient and elevated temperature, good thermal fatigue strength to resist repeated thermal cycles, good fracture toughness to resist the damage during plunging and dwelling, low coefficient of thermal expansion, and good machinability for manufacturing complex features on the shoulder and probe [22].

1.8.3. Tool Geometry

The tool geometry is a critical parameter in FSP, as it determines the heat generation, material flow, and deformation in the material. The tool geometry can be optimized based on the specific requirements of the material being processed and the desired microstructure and properties of the resulting composite, Figure 1.3 commonly, the shoulder of tool having concave shaped profile is used as it serves as an escape volume or reservoir for the displaced plasticized material from the probe [23].

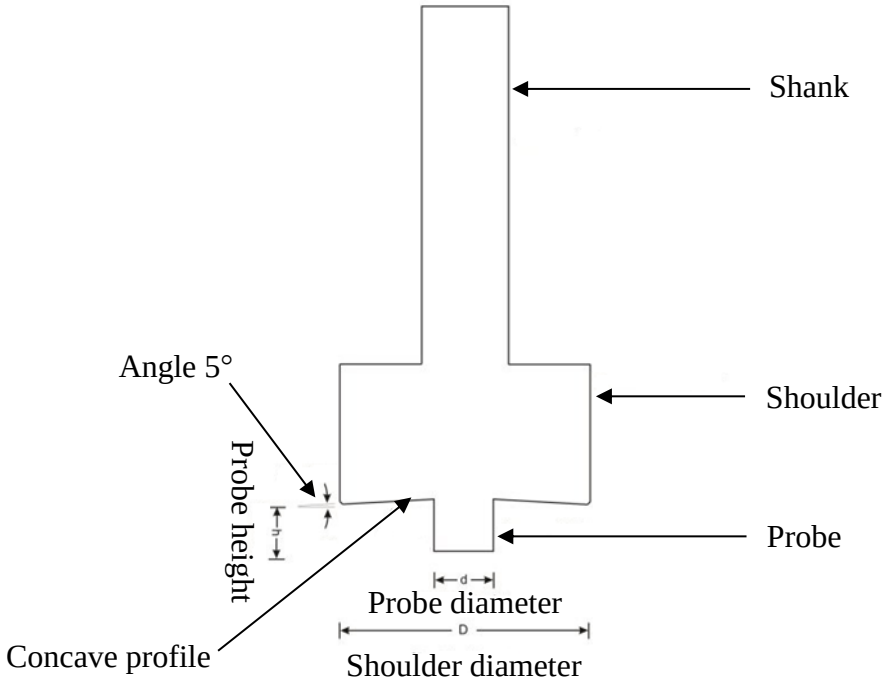

Figure 1.3. Tool geometry of FSP tool

1.8.4. Rotational Speed

The rotational speed of the tool is the most critical parameter in controlling the mechanical properties and microstructure of the friction stir processing and samples. Careful selection of the rotational speed is necessary to achieve defect-free, high-strength surface processing [24].

1.8.5. Surface Producing

There are several methods to prepare the surface for the FSP, based on the experiences of researchers during the last two decades groove FSP, hole FSP which has three types (zigzag hole method, hole method with an offset line of holes and deep hole drilled under the surface), sandwich and direct FSP [25].

1.8.5.1. Groove FSP

The groove method is a dominant solution for reinforcing composites, the groove method is the most widely adopted technique for incorporating the reinforcing phase into a matrix. Its popularity can be attributed to its early adoption, which allowed it to establish a strong foothold in the field. From the beginning, no alternative methods could match its efficiency and versatility, which led to its widespread use.

This method includes three distinct stages, first, groove formed into the plate, after that, filled the reinforcing material into the groove, finally, closed the groove using a pinless tool. These procedures creating a strong and durable composite requires a careful approach to incorporating the reinforcing materials into the matrix. One such method involves using a pin tool to distribute particles within the matrix [26].

1.8.5.2. Hole FSP

This method consists in separating the walls of individual chambers that protects the powder more effectively than the groove method. This prevents uncontrolled movement of the reinforcement stage outside the processed area. As a result, holes

closed without the need for a pinless tool after plate machining process. The process becomes a one-step process, requiring only a pin tool. Another advantage of this method is the ease of controlling the target share of the reinforcement phase in the processed material. This can be achieved by choosing the dimensions and arrangement of the holes, as well as the thickness of the walls separating them. This method also has some drawbacks. It takes longer time to prepare the sample compared to the groove method, as creating holes and filling them during the reinforcement stage is a laborious process and more time-consuming. It is important to consider the thickness of the walls that's separating the individual holes. If the walls are too thick, this may produce a localized zone with a low percentage of reinforcement stage in that zone. To mitigate this problem, an additional pass or several passes can be made to eliminate irregularities in the boost phase particle distribution. In conclusion, this method provides a controllable and convenient way to incorporate reinforcement particles into a matrix material [25].

Zigzag Hole Method

This method is considered as a new way to strengthen composite materials, and it is a unique technology used to strength. The reinforcement additive material is placed along the direction of tool movement, creating a series of holes within the composite. The researchers have discovered that a more uniform reinforcement distribution of the phase can be achieved using this method [27].

Hole Method with an Offset Line of Holes

This method provides significant benefits in terms of processing efficiency. The axis of the moving tool is displaced by a certain amount relative to the axis of the holes. The tool pin does not fully sink into the chambers filled with the hardening particles, but instead only partially interacts with the powder-filled hole. This offset arrangement allows for more efficient processing, as the interaction of the tool with the reinforcement molecules is more controlled and targeted. By avoiding complete sinking of the tool in holes filled with a powder, the process can be optimized to achieve better material integration and improved mechanical properties [28].

Deep Hole Drilled under the Surface

This method offers many benefits, including the ability to perform processing in one step using only one tool. The location of the hole under the surface ensures that the reinforcement material remains stable and is not affected by uncontrolled movement outside the processed zone. This technology provides a unique solution for reinforcement material, allowing precise control of the process. And it also has some limits. The shape and maximum length of the piercing are restricted, which may affect its overall effectiveness. Typically, these holes are created using long drilling techniques or electrical discharge machining (EDM). Despite these limitations, this method provides a promising way to process materials [29].

1.8.6. Sandwich FSP

This method is a distinct method of material reinforcement that differs from traditional methods such as the hole or groove method. This method does not create holes or grooves. Instead, the reinforcement material is placed directly to the surface of the processed sample, which is then covered with a fin layer or sheet of sample material. This sandwich assembly is then processed using the pin tool in FSP [30].

1.8.7. Direct Friction Stir Processing

This method offers new ways to enhance materials in the processing area. Unlike FSP methods, direct friction stir processing (DFSP) tools feature an internal channel that delivers the reinforcement phase directly to the processed area through gravity or additional force. This internal channel acts as a reservoir for the reinforcement material, eliminating the need to create holes or grooves and fill them with reinforcing material. This simplified process offers significant advantages over other methods [31].

The Aim of the Work

Study the visual and mechanical properties of Al 7075 - T73 after using friction stir processing (FSP) reinforced withY_2O_3 nano powder.

PART 2

LITERATURE REVIEW

As we look to the future, the work done in the past will continue to shape the direction of FSP. By drawing on the knowledge and experience gained, researchers can improve the process and unleash its full potential, ultimately leading to more innovative and sustainable solutions.

2.1. FRICTION STIR PROCESSING

The literature discusses how FSP can enhance the properties of surface composites. Researchers have achieved enhancements in microhardness by adding reinforcing particles, like ceramics or metals to the processing material. The improved hardness is typically linked to the distribution of these particles, which boosts the materials strength and durability, against wear [32].

Prabhakar et al. (2022) In this study, friction stir methods encompass a variety of processes that utilize friction as a heat source, for welding shaping or adding materials. They offer an alternative to fusion based systems for working with alloys and other materials. The seven main types of friction stir techniques include additive friction stir deposition (AFSD) friction stir additive manufacturing (FSAM) friction stir welding (FSW) friction stir processing (FSP) friction surfacing (FS) friction stir spot welding (FSSW) and friction stir lap welding (FSLW). Key control parameters, across all these techniques are force, rotational speed and welding or travel speed. Additionally, the quality of the weld is influenced by tool profiles and dimensions. The article presents an overview of the benefits, constraints and future prospects associated with these methods. It delves into the underlying principles of operation and the process parameters that impact the quality of the product [33].

Mishra et al. (2000) The authors note that traditional superplastic forming of aluminum alloys is limited by slow strain rates and requires complex thermomechanical processing to achieve fine grain sizes necessary for superplastic deformation. Previous methods achieved an optimum superplastic strain rate of practical applications in industries such as automotive manufacturing. The study utilized a 7075-T651 Al plate and applied FSP to create a fine-grained microstructure in a single pass. The microstructure analysis showed a grain size of 3.3±0.4μm, and the stress-strain behavior indicated that the material could achieve high elongation at high strain rates, with ductility ten times greater than 1000% at the optimum conditions. Mishra believes that utilizing FSP is a method to trigger strain rate superplasticity, in Al alloys, which could lead to streamlining manufacturing procedures such as casting, friction stir processing and superplastic forging or forming. The findings indicate that achieving superplasticity, in Al segments directly from structures through FSP is possible [34].

Butola et al. (2021) The study findings indicated that including reinforcing SiC powder caused a decline in the strength and flexibility of the Al 7075 matrix. Nevertheless, this decrease in characteristics was balanced out by enhancements in microhardness and resistance to wear. A tool rotational speed of 1000 rpm exerted a significant influence on the properties of the composite leading to increased microhardness and wear resistance compared to the lower speed of 700 rpm [35].

Iwaszko et al. (2021) This detailed investigation explores the advancements in surface engineering using friction stir processing (FSP). FSP technology has transformed how engineers alter material microstructures and create surface composites. The research examines approaches to incorporating reinforcing phases into the matrix, such as groove, hole and direct friction stir processing. These techniques offer a variety of advantages including controlled production of microstructures. The review discusses the pros and cons of each approach along with their limitations. By grasping these nuances engineers can choose the method for their specific requirements harnessing the flexibility and effectiveness of FSP technology. The article underscores the importance of these techniques in surface

manufacturing demonstrating FSPs potential across various industries. Through mastering the intricacies of FSP engineers can uncover opportunities for material modification that enhance engineering materials performance and durability [25].

Ding et al. (2016) In this research study, the researcher used a technique to create a composite layer by employing the groove method and tool movements. This new method involved filling a groove with reinforcement material and then moving the tool across it. The researchers introduced TiO_2 particles using this method. With a twist, the grooves were positioned perpendicular to the tool's direction. This fresh approach enabled them to produce a layer with a microstructure shedding light on both the advantages and limitations of this process. By examining how groove orientation and tool movements impact the properties of the composite this study offers insights for engineers looking to enhance surface manufacturing. The utilization of the groove method and tool movements shows potential for creating surface composites tailored to properties. By mastering this technique researchers can design materials that deliver performance and durability unlocking opportunities for diverse industrial applications [36].

Karash et al. (2015) In this research, authors focus on (FSP) and using it to enhance the surface properties of Al alloy. They investigate the impact of tool rotational and travel speeds on surface topography, hardness, microstructure and mechanical properties of the Al alloy. The diameter of 20 mm of cylindrical tool, travel speed of 60 mm/min and rotational speed of 800 rpm, for all FSP processes. The researchers found that in the friction processes the will hardness increases with cutting depth, with a significant increase in hardness rigidity with two passes compared to one. Additionally, the grain size decreased with the cutting depth, and the ratio of grain size and friction was higher for the two passes compared to the single pass.

The researchers utilized an FSP tool made from steel with specific dimensions for the shoulder and pin diameters. Various experiments on different Al alloys were conducted to analyze the effects of FSP, showing improvements in microstructural changes, ductility enhancement and wear resistance [37].

Dawood et al. (2015) The researchers investigate the impact of different tool pin profiles on the microstructures and mechanical properties of Al alloy joints using FSW. Three tool pin profiles were investigated: threaded tapered square, cylindrical, and triangular. They found that the triangular tool pin profile produced the best mechanical and metallurgical properties, while the square tool pin profile shows the lowest microhardness and tensile strength. The difference in tool pin profiles that influence on the weld joints significantly and effect on the properties like fracture behavior and grain size. The research focused on the achieving defect-free with smooth surfaces in (FSP) of Al alloys and how importance of the geometry of tool pin [38].

Jebur et al. (2021) In this research focused on the solid-state technique for modification of microstructural using the heat generated from friction and stirring. The researcher focuses on the use of SiC particles to promote grain refinement and increase of properties of hardness in the Al alloy 7075. The FSP process resulted in a hardness of 83.67 HV, which was higher than the base material 71 HV. The SiC particles showed fine grains even at elevated temperatures, leading to a pinning effect by the SiC for FSP Al 7075 particles. The application of FSP is considered effective for the mechanical improvement of semi-solid metal Al alloys. The rotational speed 1120 rpm were travelling speed set at 20 mm/min [39].

Mouli et al. (2017) In this study the researchers focus on the mechanical properties' enhancement of Al alloys, specifically Al 7075, using FSP. This technique involves localized plastic deformation by using a tool which is non-consumable to generate heat and stirring in the workpiece. The tests led to an improvement in grain refinement of Al 7075 and increased properties of hardness. The results showed that the hardness of the processed material was significantly higher than the base material, indicating the effectiveness of FSP in mechanical properties enhancement the of Al alloys, The study highlighted the importance of FSP in modifying the microstructure of Al alloys, leading to improved specific strength, used rotational speeds of 1120 ~ 1200 rpm and travel speeds of 20 ~ 80 mm/min. High of travel and

rotational speeds increased heat input, which affected on particle distribution in the SZ, surface roughness, grain size [40].

2.2. COMPARISON BETWEEN FRICTION STIR PROCESSING and OTHER SIMILAR PROCESSES

Friction stir processing is a microstructure modification technology of solid-state process which is similar to friction stir welding in terms of principles and process. Both FSW and FSP involve severe plastic deformation of materials at temperatures below the melting point [41].

2.2.1. Laser Surface Processing

Laser surface processing (LSP) is a cutting-edge technique that leverages high-powered laser beams to transform the surface of materials. This process involves melting the surface layer of the material, which then solidifies, yielding distinctive microstructures and compositions. The fast-cooling rates involved in this process can produce microstructures that are not attainable through traditional surface treatment methods. This technique can be applied to enhance the properties of a broad range of materials, including Al alloys, by inducing microstructural changes and properties improving such as hardness, wear resistance and corrosion resistance [42].

2.2.2. Laser Beam Machining

Laser beam machining (LBM) is an innovative thermal machining process utilizes laser beams to generate heat flux melting and vaporizing the workpiece material for machining of intricate shapes, in different materials. One of its advantages is its contact nature eliminating physical contact between the tool and workpiece reducing tool wear and tear and enabling automated machining. Moreover, this method creates a heat affected zone, preserving material properties and ensuring the product retains its original characteristics. The versatility of this process allows it to be applied to materials such as alloys, non-metals and composite materials making it appealing for

industries requiring precise machining of complex components. Overall, this technique combines precision, speed and adaptability effectively for industries that need machining of shapes, in diverse materials [43].

2.2.3. Plasma Arc Welding

Plasma arc welding (PAW) is a welding technique that utilizes a high temperature plasma arc to melt and connect metal components. It is commonly used for welding thick sections of steel and other metals. However, the equipment used for plasma arc welding is intricate and expensive and the requirement for water cooling the torch restricts how compact the torch can be designed [44].

2.2.4. Shot Peening

Shot peening is a cold surface treatment that involves projecting small spherical beads called shot at high velocities several m/s onto a workpiece to induce compressive residual stresses on the surface. The repeated impacts cause plastic deformation of the workpiece, which improves its mechanical characteristics by increasing resistance to fatigue and corrosion, by allowing the treatment of complex geometries by using a shot peening technique.

Shot peening is a widely used surface treatment that improves the mechanical properties and fatigue life of components by inducing beneficial compressive residual stresses on the surface. The treatment involves projecting small spherical beads at high velocities onto a workpiece, causing plastic deformation and improving resistance to fatigue and corrosion. The quality of the treatment is dependent on the impact features, and the use of a polymer material chamber can reduce the average depth of marks [45].

2.2.5. Electrochemical Machining

Electrochemical machining (ECM) is a cool way to shape and cut metal parts without using traditional machining methods. Instead of relying on heat, pressure, or

mechanical force, ECM uses electricity and a special liquid solution to dissolve away the unwanted parts of the workpiece. Here's the process; First the workpiece becomes the electrode (anode) in a cell. Next a tool, with a charge (the cathode) is brought near the workpiece. When electricity is applied, the workpiece material dissolves into the solution allowing the tool to shape the part as desired. An interesting aspect of ECM is its nature. Because there’s no cutting force or heat involved it's ideal for crafting parts or dealing with materials that are challenging to machine using methods. Additionally, it excels at producing 3D shapes and detailed surface features that may be hard or impossible to achieve with machining techniques.

This method represents an approach to shaping metal components using only electricity and a bit of chemistry. It stands out as a precise and adaptable process [46].

2.2.6. Electrical Discharge Machining

Electrical discharge machining (EDM) method is a machining technique that uses discharges or sparks to carve out material from a workpiece. This innovative process involves generating a controlled discharge, between an electrode and the workpiece producing energy that melts and wears away the material. EDMs exceptional capabilities make it ideal for shaping forms and tough materials that are hard to work with using methods. One of the benefits of EDM is its efficiency in handling shapes and sturdy materials. Its flexibility makes it an asset across sectors such as aerospace, automotive and medical device production. The precision and accuracy of EDM also allow for the crafting of designs and features that would be challenging or impossible to achieve through machining techniques.

This method provides an effective approach for working with intricate materials proving to be valuable across various industries. Its precision in crafting designs and features distinguishes it from alternative machining methods positioning it as a resource for manufacturers aiming to manufacture top notch components, with intricate shapes [47].

2.2.7. Ultrasonic Machining

Ultrasonic machining (USM) technique involves a method of machining that utilizes high frequency vibrations to eliminate material from workpieces. This method works well for working on materials such as ceramics, glass and silicon without causing any heat or strain. It includes placing a tool tip in a mixture and using high frequency vibrations to move the tool, which then directs the particles towards the object being worked on eroding material through focused abrasion. Ultrasonic Machining adaptability makes it a valuable technique, for uses. Its precision and control features make it especially ideal for industries that require levels of accuracy, like aerospace, electronics sectors [48].

These processes, like FSP, are used to modify the properties and microstructure of materials, but there are differences in mechanisms and applications of their process, While FSW and FSP share some similarities. So, for joining two pieces of metal can use FSW, whereas to modify the properties of a single piece of material will use FSP. The main objective of FSW is used to join materials, whereas FSP is to alter the microstructure of the material [49].

2.3. BENEFITS and CHALLENGES of METAL MATRIX COMPOSITES

FSP can produce a refined grain structure in the matrix, leading to enhanced mechanical properties like modulus, hardness, and tensile strength, also improve the distribution of reinforcement particles, resulting in better wear resistance and reduced coefficient of thermal expansion, and it is a solid-state process that does not involve melting, which reduces the likelihood of distortion and defects in the material, and it can be used to join metal matrix composites (MMCs) in a reliable manner, overcoming the challenges associated with conventional fusion welding techniques [50, 51].

In the other hand wear down quickly, which can affect the quality of the processed material, The processing parameters such as tool speed, rotational speed, and number

of passes need to be optimized to achieve the desired microstructure and properties, it can be a time-consuming and expensive process, especially for large-scale production. FSP offers significant benefits for MMC, including properties improved and distortion reduced. However, it also presents some challenges related to the tool processing parameters, wear and scalability [52].

2.4. EFFECT of YTTRIUM OXIDE ADDITION on MICROSTRUCTURE and MECHANICAL PROPERTIES of Al ALLOYS

Researchers have explored ways to optimize the grain refining process and mechanism of Y_2O_3 in combination with Al alloys to maximize the benefits of FSP. This focus has continued in recent years, driven by the need to improve the overall performance and efficiency of FSP.

Kumar et al. (2023) In this study the researchers focused on the influence of rare earth elements, especially Y_2O_3, on the mechanical properties and microstructure of AMMCs. It highlights the Y_2O_3 effect on mechanical properties and microstructure of MMCs. Y_2O_3 addition to aluminum alloys like AA6082 and AA7075 leads to significant improvements in yield strength (YS), ultimate tensile strength (UTS), and elongation. Incorporating 9 vol.% Y_2O_3 into AA6082 using friction stir processing resulted in a 45.45% increase in UTS, 43.17% increase in YS, and 33.33% increase in elongation. A composite of AA7075 with 10 vol% Y_2O_3 prepared by high-energy ball milling for 20 hours achieved a maximum hardness of 260 HV. While he studies the effect of Y_2O_3 on microstructure of AMMCs, the distribution of Y_2O_3 particles in AMMCs and the formation of intermetallic compounds like $Al_5O_{12}Y_3$ and Al_3Y contribute to the enhancement of physical properties. Agglomeration of Y_2O_3 particles above 10 wt.% can lead to a decline in the strength of the composites due to weakening of the internal structure. The formation of the Al_3Y phase and microstructure modification in Al-20 wt.% Y_2O_3 samples improved hardness, polarization behavior, and wear resistance. In summary, the incorporation of Y_2O_3 into aluminum alloys, particularly AA6082 and AA7075, significantly enhances their mechanical properties and microstructural characteristics, making them suitable for various applications [53].

Joshi et al. (2024) The study investigated the behavior of dry sliding wear of AA-7075 AAMC reinforced with micrometric and nanometric yttrium oxide (Y_2O_3) particles, fabricated by sinter-forging and powder metallurgy. The composites were artificially aged to peak hardness. Composites with nanometric Y_2O_3 showed lower overall wear compared to micrometric Y_2O_3 at the same volume fraction. The material strengthening by precipitation hardening and uniform distribution of Y_2O_3 particles improved wear resistance. Wear mechanisms consisted of adhesive wear with plastic deformation followed by abrasive wear because of hard reinforcement particles. Coefficient of friction (COF) was slightly lower for composites with higher micrometric Y_2O_3 content at 10N load, but similar at 20N and 30N loads. The wear rate decreased with increasing micrometric Y_2O_3 up to 5 vol% at 1 m/s, and up to 10 vol% at 2 m/s sliding speed. Worn surfaces showed wear grooves, delamination, plastic flow and loose wear particles, with more uniform wear for composites with lower Y_2O_3 contents. The results demonstrate that nanometric Y_2O_3 reinforcements provide better wear resistance compared to micrometric Y_2O_3 in AA-7075 aluminum matrix composites processed by powder metallurgy and sinter-forging [54].

Lin et al. (2024) They study the addition of rare earth elements like yttrium (Y) to pure aluminum alloys can significantly improve their strength and electrical conductivity. Yttrium additions refine the grain size of cast aluminum alloy, containing second phases heterogeneous nucleation sites and pin grain boundaries, contributing to the grain refinement modify the morphology and composition of the Fe and Si containing impurity phases, reducing their harmful effects on the matrix, exhibits high strength, high electrical conductivity and good elongation simultaneously, overcoming the inherent contradiction between strength and conductivity in aluminum alloys, In summary, aluminum alloys with yttrium additions exhibit improved strength, electrical conductivity, and impurity resistance, making them ideal for a wide range of applications including automotive components, electrical conductors, and structural materials where a balance between strength and conductivity is essential [55].

PART 3

EXPERIMENTAL STUDIES

3.1. MATERIALS and CHEMICAL CONTENTS

3.1.1. Aluminum alloy 7075-T73

In this study, aluminum alloy Al 7075-T73 was used as base materials. The raw plate used for processing is obtained from the market.

3.1.2. Tool Selected

The tool used in this process was made from KS SKH 51 type has an unthreaded cylindrical 16.5 mm shoulder diameter, having cylindrical pin length of 2.7 mm and pin diameter 4 mm shown in Figure 3.1.

Figure 3.1. Tool Steel KS SKH 51 type for FSP

3.1.3. Chemical composition of the Al 7075 plate and the tool

The chemical contents of the processed Al 7075-T73 are shown in Table 3.1, and the tool chemical composition shown in Table 3.2, by the chemical analysis spectrum device Figure 3.2 belonging to the laboratory of State Company for Inspection and Engineering Rehabilitation (SIER) / Baghdad, as shown in Figure 3.3 SIER certificate. While Tables 3.1 and 3.2 give general element distributions, all element distributions are given in Figure 3.3.

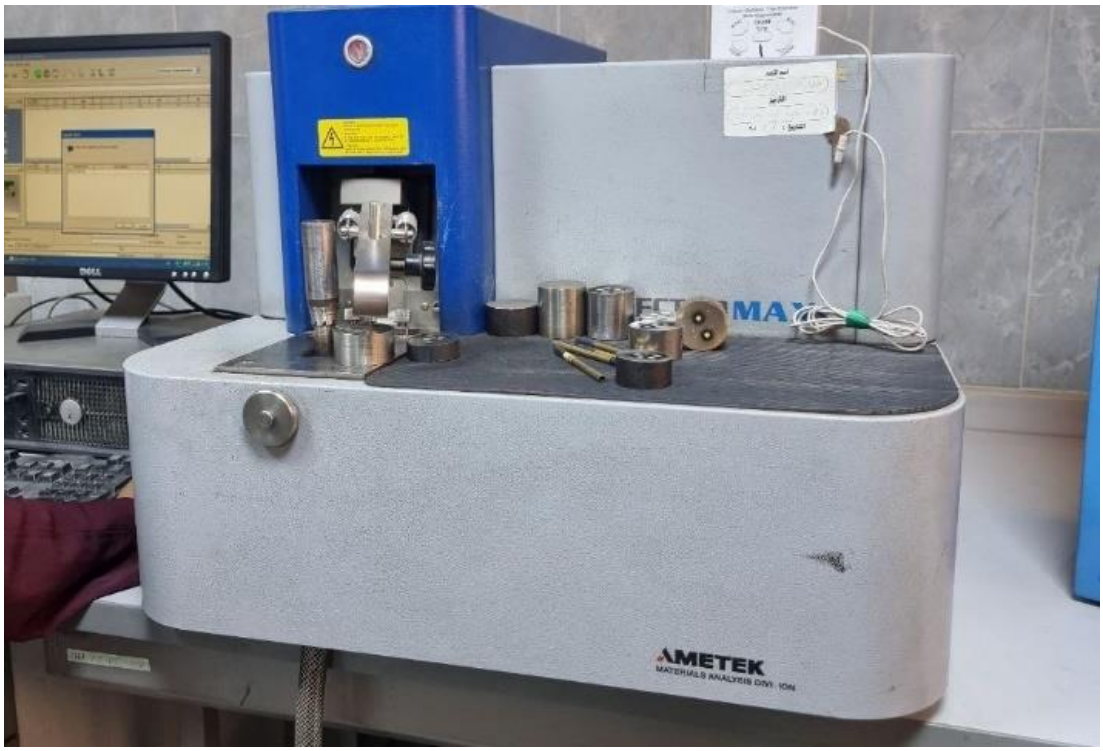

Figure 3.2. METEK spectrum device

Table 3.1. Al 7075-T73 plate chemical composition (%)

Sample	Type	Si	Fe	Cu	Mg	Cr	Ni	Zn	Ti	Al
Al Plate	AA 7075	0.069	0.500	1.35	2.62	0.280	0.085	6.1	0.0817	Bal.

Table 3.2. Tool steel chemical composition (%)

Sample	Type	C	Mn	Cr	Mo	Ni	Co	V	W	Fe
Steel Shaft	KS SKH 51	0.852	0.270	4.19	5.19	0.259	0.443	1.63	6.7	Bal.

Figure 3.3. Certificate and test report of Al plate and tool shaft
(a) type of material certificate (b) chemical composition test report

3.2. PROCESSES PREPARATIONS

3.2.1. Plates

Al 7075-T73 plates dimensions of 200 x 100 x 3 mm was prepared shown in Figure 3.5 using Hiraoka model cutting machine in Diyala university / mechanical department laboratory shown in Figure 3.4.

Figure 3.4. Hiraoka cutting machine

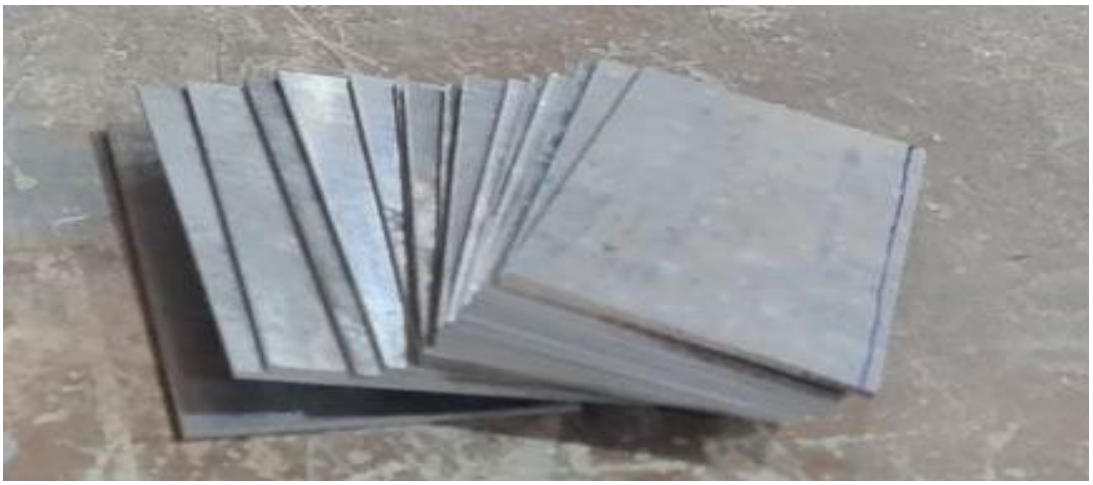

Figure 3.5. Plates after cutting

3.2.2. Groove

The groove done at 45° as V shape with dimensions 2 mm width 1.5 mm depth by machining tool was made after cutting the Al 7075-T73 plates by JAFO milling machine in Musayyib Thermal Power Plant Workshop as shown in Figure 3.6 for adding Y_2O_3 to enhancement the Al 7075-T73 mechanical and physical properties.

Figure 3.6. V - Groove machining

3.3. FRICTION STIR PROCESSING

The Al 7075-T73 surface was processed with Y_2O_3 nano particles. Al 7075-T73 plates of 200 x 100 x 3 mm reinforced with Y_2O_3 particles in nano size 40 nm were used for experimentation. Friction stir processing was made on the Al 7075-T73 plates by using JAFO milling machine as shown in Figure 3.7.

Figure 3.7. JAFO milling machine

The base plate of fixture is 400 mm in length, 300 mm in width, 15 mm thick and 20 mm thick plate is used as the plate holder, all made from mild steel as shown in Figure 3.8.

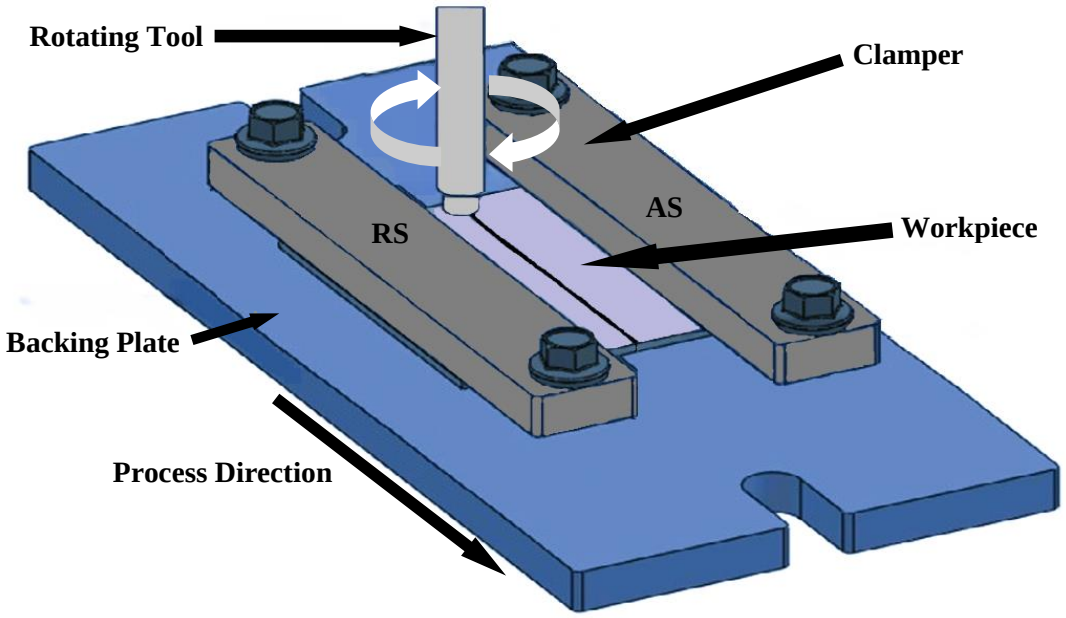

Figure 3.8. Schematic diagram of experimental setup in the friction stir processing

An unthreaded cylindrical tool with 16.5 mm shoulder diameter, having cylindrical pin have length of 2.7 mm and 4 mm tool pin diameter was made from tool steel KS SKH 51 used in the process the end of the pin was cylindrical as shown in Figure 3.9.

Figure 3.9. Unthreaded cylindrical FSP tool

So that, the V-groove was made to apply the Y_2O_3 particles on the surface of the Al 7075-T73 plate to prevent it being thrown outside of the stir zone as shown in Figure 3.10. below.

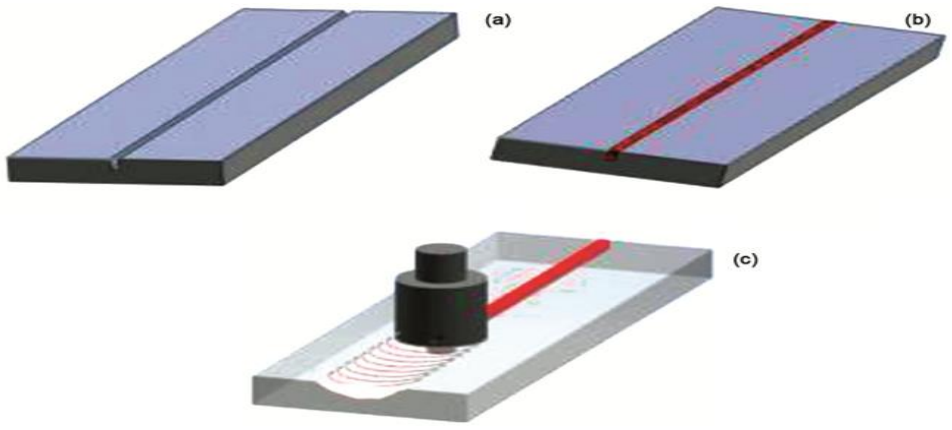

Figure 3.10. FSP operational overview (a) V groove machining, (b) Y_2O_3 inserting to the groove (c) start FSP [19]

Various microstructural zones are formed during the FSP and the same is shown in Figure 3.11. The stir zone or can called nugget zone (NZ), thermo-mechanical affected zone (TMAZ), heat-affected zone (HAZ), and base material (BM).

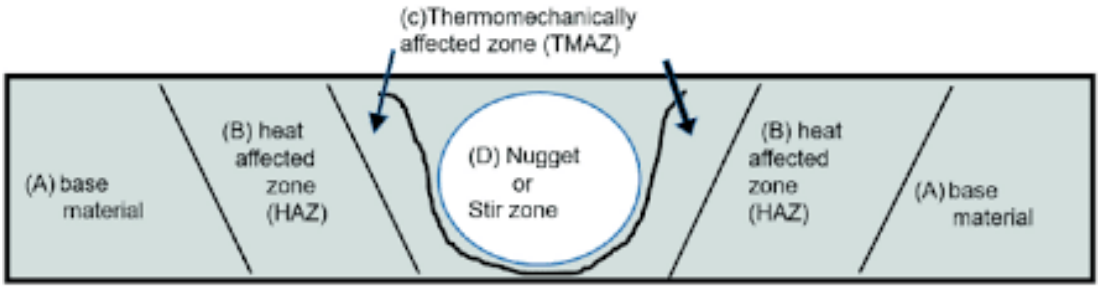

Figure 3.11. Transverse schematic section of the specimen [56]

In the Table 3.3 shows the various process parameters conditions applied in this research. with different rotational speeds ranging from 710, 900 and 1120 rpm clockwise, transvers speed ranging from 55, 70 and 90 mm/min from left to right side across the roiling direction with tilt angle 2° of the tool and shoulder plunge depth of 0.2 mm were used for friction stir processing applying yttrium oxide (Y_2O_3) nano particles.

The dwell time was given 10 sec and 0.2 mm offset was taken for friction stir processing. Parameter selection of friction stir processing is a critical task to obtain defect free by using the vertical milling machine. This depends upon the tool geometry, tool material and material to be processed.

In the current research work, different conditions were applied for 9 conditions and found out the optimized processing conditions by observing the visual and mechanical inspection for the specimens.

Table 3.3. FSP test parameters.

Sample No.	Rotational speed rpm	Travel speed mm/min	Sample No.	Rotational speed rpm	Travel speed mm/min	Sample No.	Rotational speed rpm	Travel speed mm/min
1	710	55	**4**	900	55	**7**	1120	55
2	710	70	**5**	900	70	**8**	1120	70
3	710	90	**6**	900	90	**9**	1120	90

According to the ASTM E8-E8M-09 [57], the tensile specimens were prepared 100 mm in length, 10 mm in width, the gauge length of 30 mm and the arc of 6 mm radius, bending specimens were prepared 100 mm in length, 10 mm in width, 3 mm height, as shown in Figure 3.12 were made by a waterjet machine.

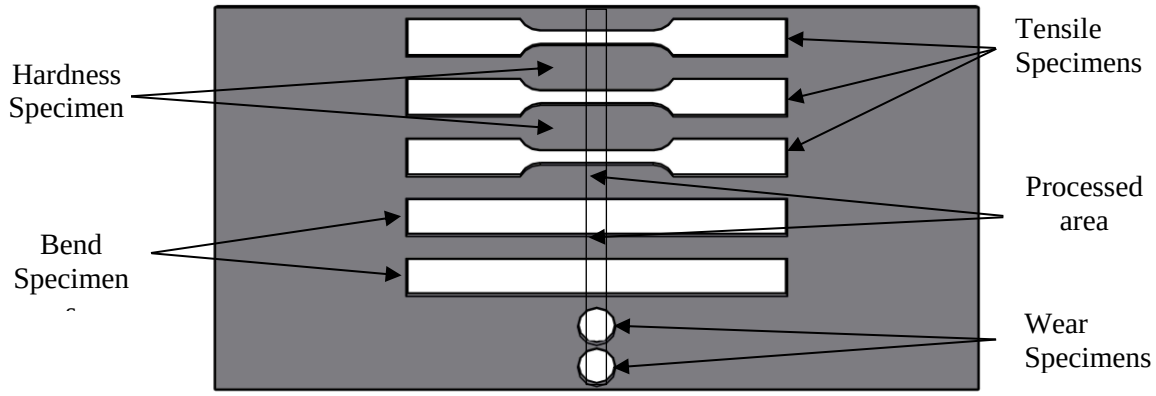

Figure 3.12. Dividing processed plates into testing specimens

The specimens for tensile and bend were tested by LARYEE machine of 100 kN Servo Hydraulic capacity 1 mm/min speed.

Wear specimens were cut out using a waterjet machine as a cylindrical shape 10 mm in diameter, 3 mm highest. It was carried out by the Dynamic Tester with a speed of 950 rpm, 10N load, distance from disk center 6.5 cm, for 5, 10, 15 minutes.

Fresh samples were cut down for hardness, OM, SEM, EDS and XRD analysis. Microstructure and dispersion of yttrium oxide particles were analyzed using an optical microscope. Specimens were cut off from the processed plate in order to observe the microstructure and dispersion of particles. For metallographic analysis, the specimens were mirror polished through proper grinding and polishing procedure. Emery paper wet grinding in grits of 400p 600p 800p 1000p 1200p According to ASTM E3 standard [58], and polishing process was carried out by using alumina suspension with a particle size of 0.3μm to achieve a proper finish. Then specimens cleaned by distilled water and ethanol, then dried with hot air. Afterward, the specimens etched by Keller's Reagent to reveal the microstructure 92 ml Distilled water, 6 ml Nitric acid, 2 ml Hydrofluoric acid, swapping the specimens for 10 ~ 30 sec to reveal the microstructure. The same procedure was carried out to observe the dispersion of yttrium oxide particles in the stir zone, TMAZ, HAZ and base material. The same procedure was used for Vickers microhardness test for the hardness of parent metal as well as stir zone, TMAZ, HAZ and base material.

The parameters used for that test were: 4.9 N 500g indentation load, 15 sec dwell time and 0.6 mm distance between two consecutive indentations.

3.4. SPECIMENS PREPARATION for ANALYSIS

The Specimens were prepared for testing Hardness, OM, SEM, EDS and XRD by placing them in a mold using a STRUERS CitoPress-10 device shown in Figure 3.13 below.

Figure 3.13. STRUERS CitoPress-10 mold maker device

It uses emery paper wet grinding in grits of 400 600 800 1000 1200 and polishing process by STRUERS Tegramin-30 grinder and polisher device in (KBU) Iron and Steel Institute / Metallography laboratory shown in Figure 3.14.

Figure 3.14. STRUERS Tegramin-30 grinder and polisher device

The specimens were carried out by using Metkon alumina suspension with a particle size of 0.3µm, then specimens cleaned by distilled water and ethanol, then dried with a hot air to prevent surface oxidization.

According to ASTM E407-3 [59] Etching: Keller's reagent was used 92 ml distilled water, 6 ml Nitric acid, 2 ml Hydrofluoric acid, swapping the specimens for 10 ~ 30 sec to reveal the microstructure then dried with a hot air to prevent surface oxidization Figure 3.15.

Figure 3.15. Specimens after etching

3.5. MICROSTRUCTURAL EXAMINATIONS

3.5.1. Optical Microscope Images

Aluminum 7075-T73 processed specimens investigated microstructure by Nikon Eclipse MA200 model optical microscope in Karabuk University (KBU) Iron and Steel Institute / Metallography laboratory shown in Figure 3.16.

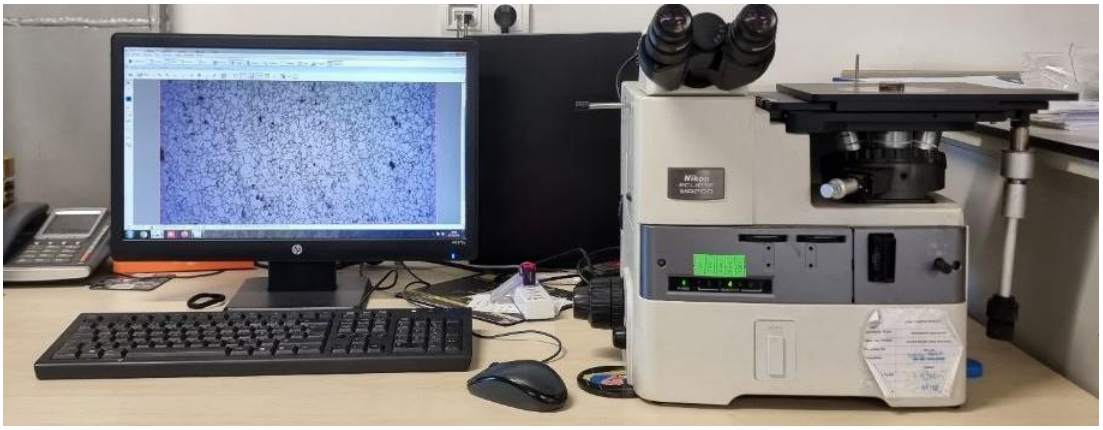

Figure 3.16. Optical microscope used for microstructure investigation

3.5.2. Scanning Electron Microscope and Energy Dispersion Spectrometry

Aluminum 7075-T73 SEM Images investigations of the produced samples in Iron and Steel Institute / Metallography laboratory (KBU), Carl Zeiss Ultra Plus Gemini FESEM model scanning electron microscope device in the laboratory Figure 3.17.

In addition, EDS analysis studies were conducted in the same SEM device. This complementary approach allowed us to gain a more comprehensive understanding of the sample's composition and structure.

Figure 3.17. SEM microstructure investigation

3.5.3. X-ray Diffraction Analysis

Malvern PANalytical AERIS model XRD devices Figure 3.18 were used to determine the chemical contents and phases-texture of the Al 7075-T73 surface processed by FSP in in the nanotechnology laboratory in Al-Khora Company / Baghdad.

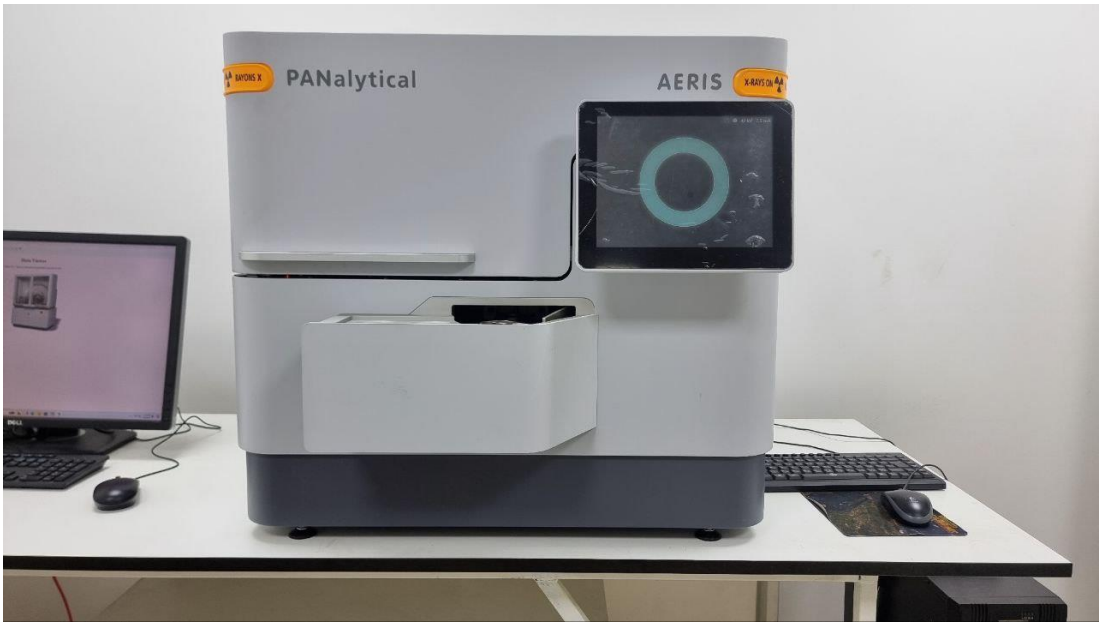

Figure 3.18. XRD device

3.6. MECHANICAL EXPERIMENTS

3.6.1. Hardness Test

Hardness test from the upper surface were carried out by LARYEE Digital Micro hardness tester shown in Figure 3.19, in the laboratory of Micro and Macro Hardness measurement / Materials Engineering department / University of Technology – Baghdad, and the hardness tests for the side surface were carried out by QNESS Q10 A+ Digital Micro hardness tester shown in Figure 3.20, in Iron and Steel Institute / Micro and Macro Hardness measurement laboratory / (KBU), based on the Vickers hardness method, using a Flat plate under 4.90N 500g load, in accordance with the TS-EN-ISO 6507 standard Vickers hardness, at least 14 measurements were taken for each Specimen [60].

Figure 3.19. LARYEE Micro hardness tester

Figure 3.20. QNESS Q10 A+ Micro hardness tester

3.6.2. Tensile Test

Tensile tests are carried out in the Materials Resistance laboratory of the Materials Engineering department, University of Technology – Baghdad, according to ASTM E8-E8M-09 standard [57]. Specimens were prepared 100 mm in length, 10 mm in width. The gauge length of 30 mm and the arc of 6 mm radius are shown in Figure 3.21.

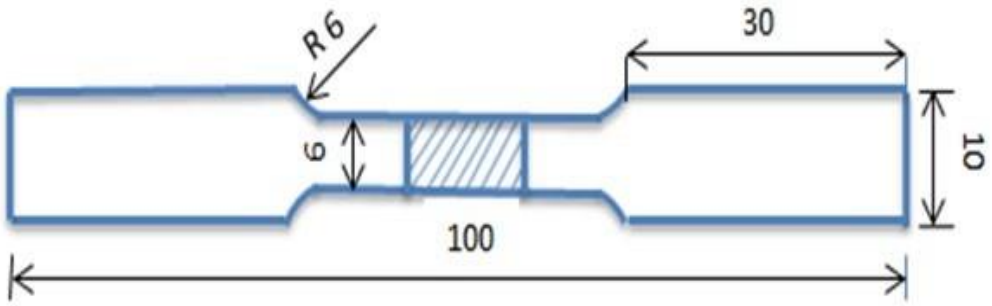

Figure 3.21. Schematic sample for tensile test (all dimensions are in mm)

At room temperature with a speed of 1 mm/min by LARYEE brand 100kN servo hydraulic. It was carried out using the dynamic tester shown in Figure 3.22. From Figure 3.23 we can see the tensile specimens before the test.

Figure 3.22. LARYEE tensile testing machine

Figure 3.23. The tensile specimens before test

3.6.3. Wear Test

Wear tests are carried out in the Materials Resistance laboratory at Materials Engineering department of the University of Technology – Baghdad, according to ASTM G99-05 pin on disk test [61]. The specimens were cut out using a water jet machine as a cylindrical shape 10 mm in diameter, 3 mm highest, Figure 3.24 shows the samples before wear test.

Figure 3.24. Wear test specimens

The pin-on-disk method for wear tests are preferably used to determine sliding wear, as Schematic shown in Figure 3.25.

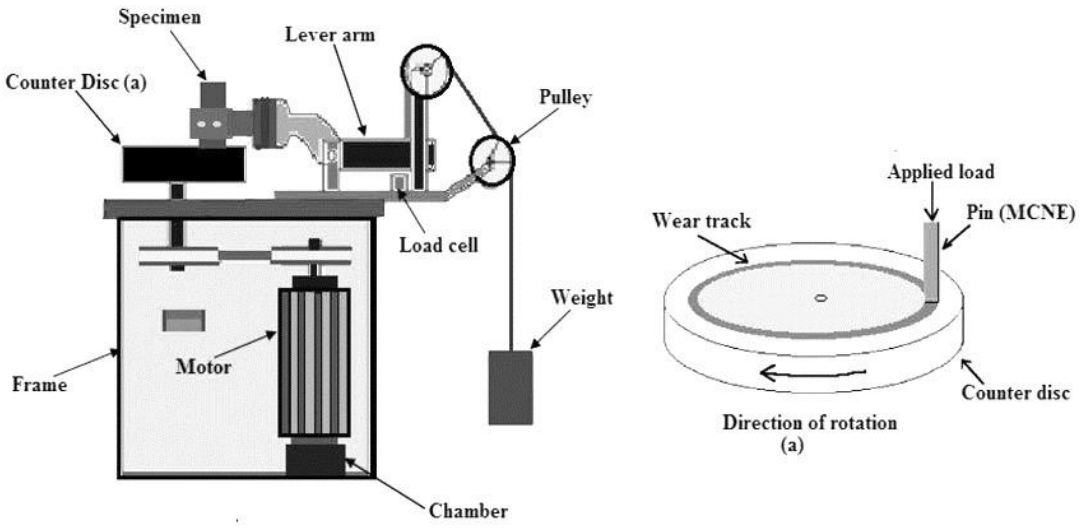

Figure 3.25. Schematic of the pin-on-disk apparatus [62]

The pin is attached with the material that is slid against the metallic disk; the disk made of tool steel material with a hardness 385 HV as Figure 3.26.

Figure 3.26. Wear testing machine

Where The Steps to conduct the wear test as below:

1. Reset delicate balance.
2. Weight the sample before and after the test with delicate balance.
3. Show the disk in the place of the ad hoc working to clean it by smoothing paper before the start of the test.
4. Fix the load, which should be perpendicular to the sample after installing it in the designated place.
5. Reset the stopwatch.
6. Turn on the device and turn on the stopwatch as well as that hour.
7. After 5 min of operation stops the device.
8. Release the sample from the device and measure the weight of the sample in the delicate balance and record the weight.
9. Fix the sample again and repeat the same previous steps and time, then arrange the different results obtained in Table 3.4.

Wear apparatus, with a speed of 950 rpm, 10N load, distance from disk center 6.5 cm, (5, 10, 15) minutes at room temperature with LARYEE brand. It was carried out using the dynamic tester.

Table 3.4. Wear results obtained from the test

Time (min)	$t_{0\,(0)}$	$t_{1\,(5)}$	$t_{2\,(10)}$	$t_{3\,(15)}$	**ΔW**	**W.R**	**S.D**
Wight (g)	W_0	W_1	W_2	W_3	**g**	**g/cm**	**m**
1 710/55	0.6382	0.636	0.6324	0.6295	0.0087	3.88	
2 710/70	0.6221	0.6209	0.6167	0.61	0.0121	5.40	
3 710/90	0.6193	0.6182	0.6152	0.6082	0.0111	4.95	
4 900/55	0.6132	0.6123	0.609	0.6032	0.01	4.46	
5 900/70	0.6248	0.6226	0.6185	0.6143	0.0105	4.60	5816
6 900/90	0.6359	0.6336	0.6289	0.6218	0.0141	6.29	
7 1120/55	0.6194	0.618	0.6147	0.6071	0.0123	3.97	
8 1120/70	0.617	0.6147	0.6114	0.6062	0.0108	4.82	
9 1120/90	0.6256	0.6236	0.6177	0.6139	0.0117	5.22	
10 Base material	0.6634	0.6611	0.6581	0.6531	0.0103	4.59	

3.6.4. Bending Test

Bending tests are carried out in the Materials Resistance laboratory of the University of Technology – Baghdad, Materials Engineering department, with LARYEE brand 100kN Servo Hydraulic capacity shown in Figure 3.30. 1 mm/min speed at room temperature, where the specimen's dimensions 100 mm in length, 10 mm width, 3 mm height according to ASTM E290-14 standard three-point bending [63]. The distance between the 2 supporting pins was 80 mm, were pin diameter 30 mm.

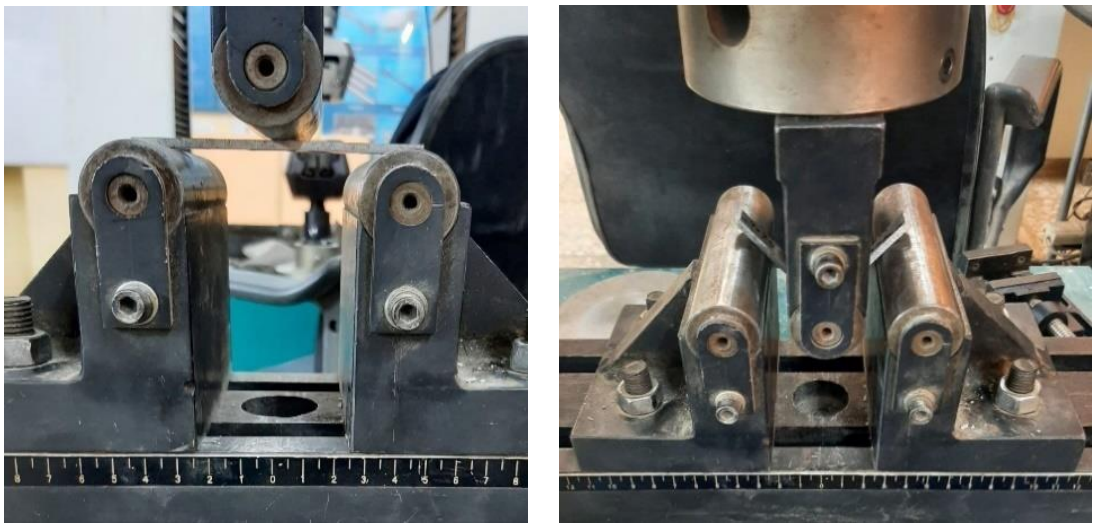

Figure 3.27. Three points bending processe

From Figure 3.27 can see three points bending process and device.

PART 4

RESULTS AND DISCUSSIONS

4.1. MICROSTRUCTURAL RESULTS

In this part, the examination for FSP microstructure OM, SEM, EDX and XRD for the processed specimens are given.

4.1.1. Optical Microscope Images Result

In Figure 4.1 provides OM of Al 7075-T73 specimen that were subjected to base material.

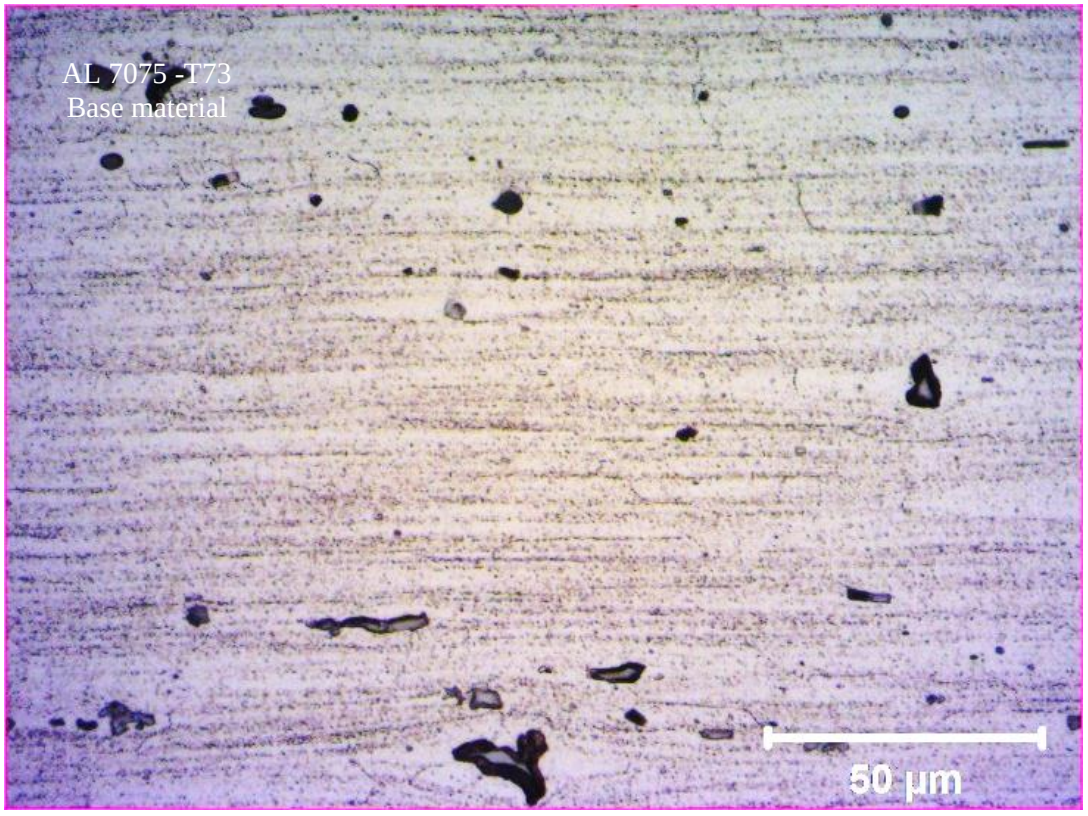

Figure 4.1. Optical microscope images of base material Al 7075-T73

In Figure 4.2. Optical microscope images are given for specimen no. 1.

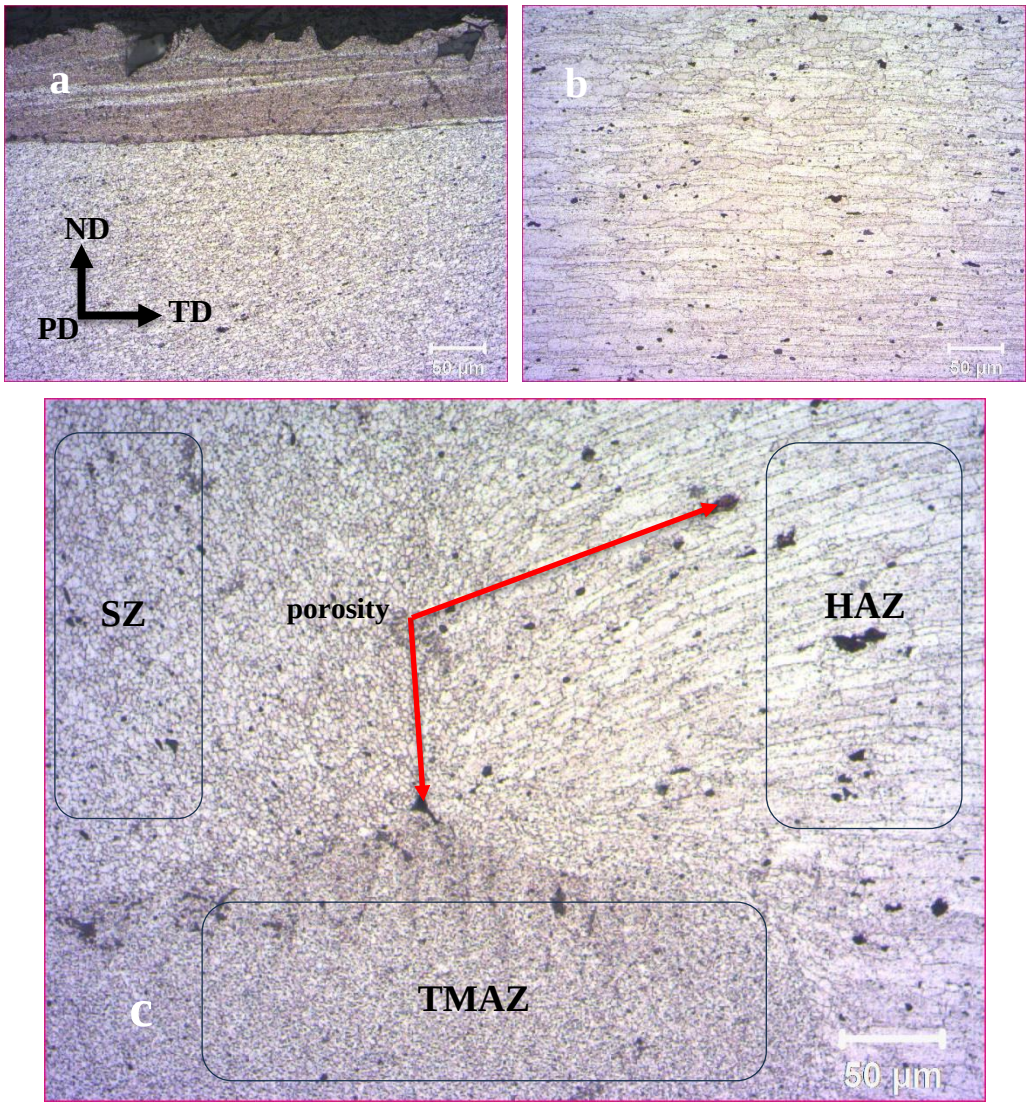

Figure 4.2. Optical micrographs of specimen no. 1

Multifocal micrographs of the transverse cross-section of Al 7075-73
ND: Normal direction, PD: Processing direction and TD: transverse direction

Figure 4.2 shows different processed zones, when fig. 4.2 (a) shows SZ area and there are some clear different layers, where the upper area represented Al particles with brown color and the other area is mixed with Y_2O_3 as fine particles.

From Figure 4.2 (b) can we see the HAZ with large size of grains, where Figure 4.2 (c) shows three zones SZ, HAZ and TMAZ.

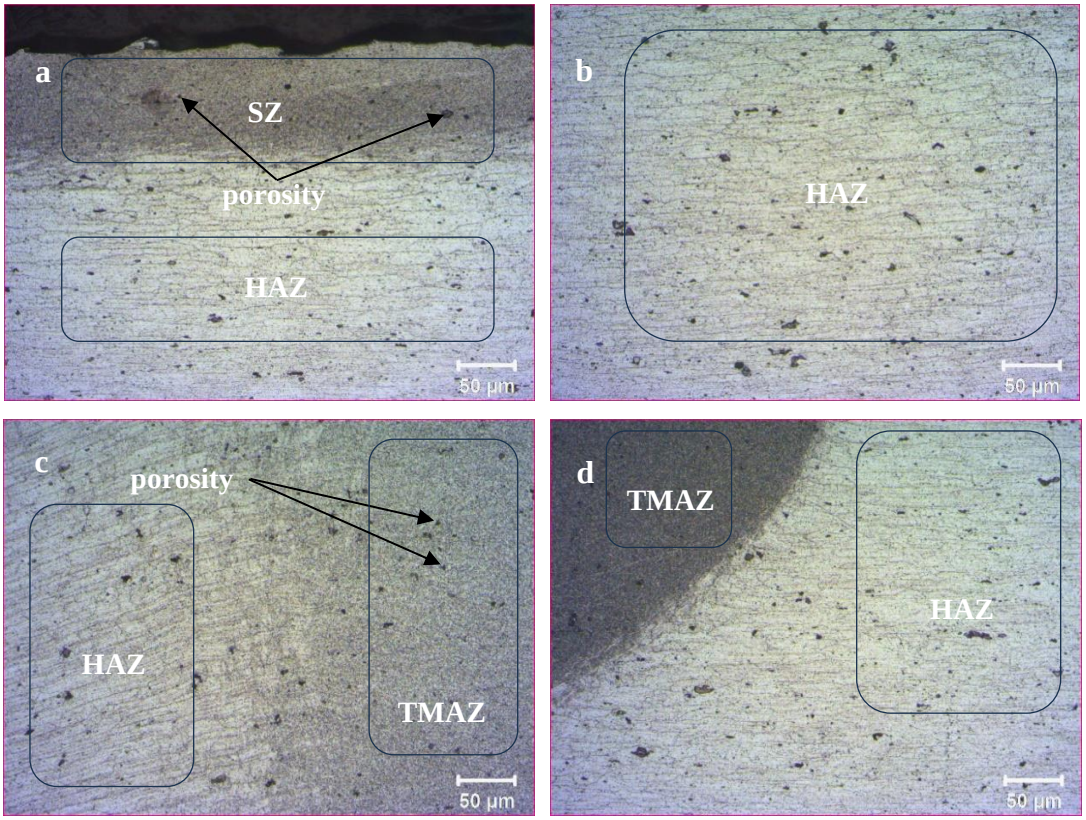

Figure 4.3. Optical micrographs of specimen no. 2

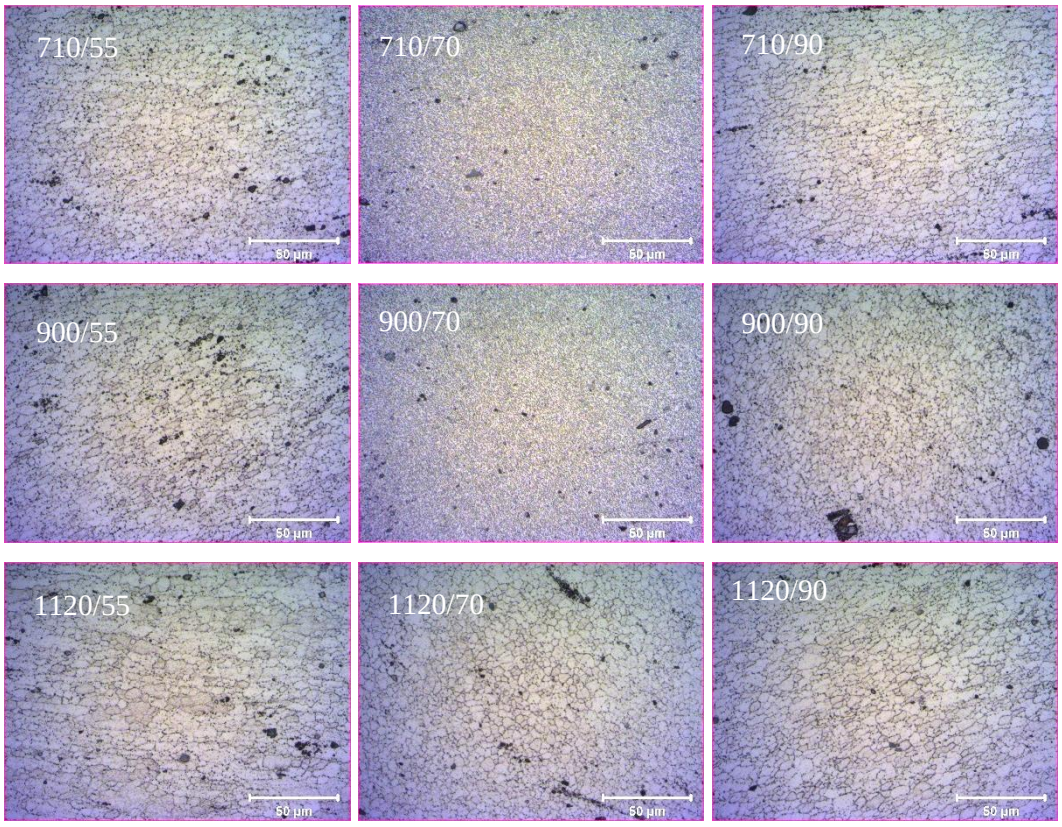

Figure 4.4. Optical micrographs of SZ

Figure 4.4. shows the microstructure of the stir zone (SZ) under different rotational speeds. All stir zones were defect free. The microstructure in the SZ was homogeneous and the grain size was highly refined relative to the base material. Grain size and precipitation behavior in the SZ could not be quantified using OM due to the fin size and there are Y_2O_3 nano particles.

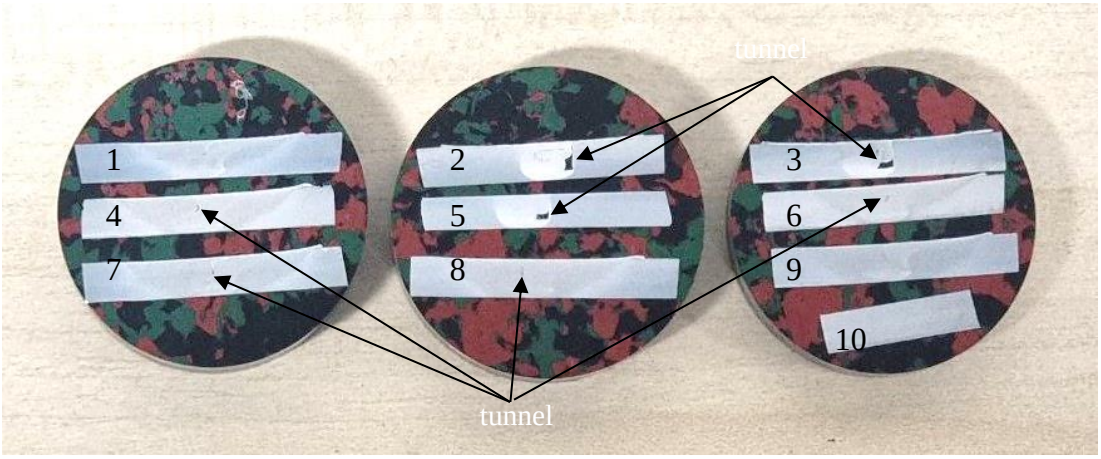

Figure 4.5. Specimens prepared for OM tests

Figure 4.5. shows all specimens after preparing for OM tests and can see by the visual eyes how specimens no. (2, 3 and 5) has a big tunnel, and the specimens no. 4,6,7 and 8 have a small tunnel, while only specimens no. 1 and 9 have no apparent deformity.

As expected, the size of particle of the SZ decreases as the tool rotational speed decreases. This is caused by the reduction of the heat input with the decrement of the tool rotational speed. As the heat input decreases [64].

4.1.2. Scanning Electron Microscopy Images Result

Examination using scanning electron microscopy (SEM) confirmed the results seen in optical micrographs SEM images of processed samples are given, for samples 3 and 6 from Figures 4.6 and 4.7 which shows SEM images of the mentioned specimens.

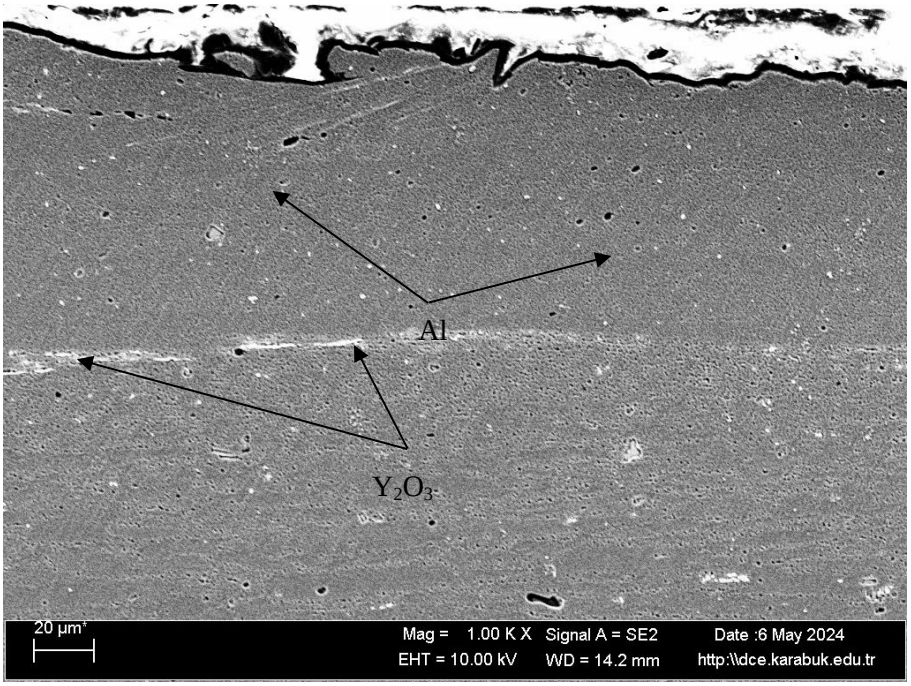

Figure 4.6. SEM images of samples no. 3

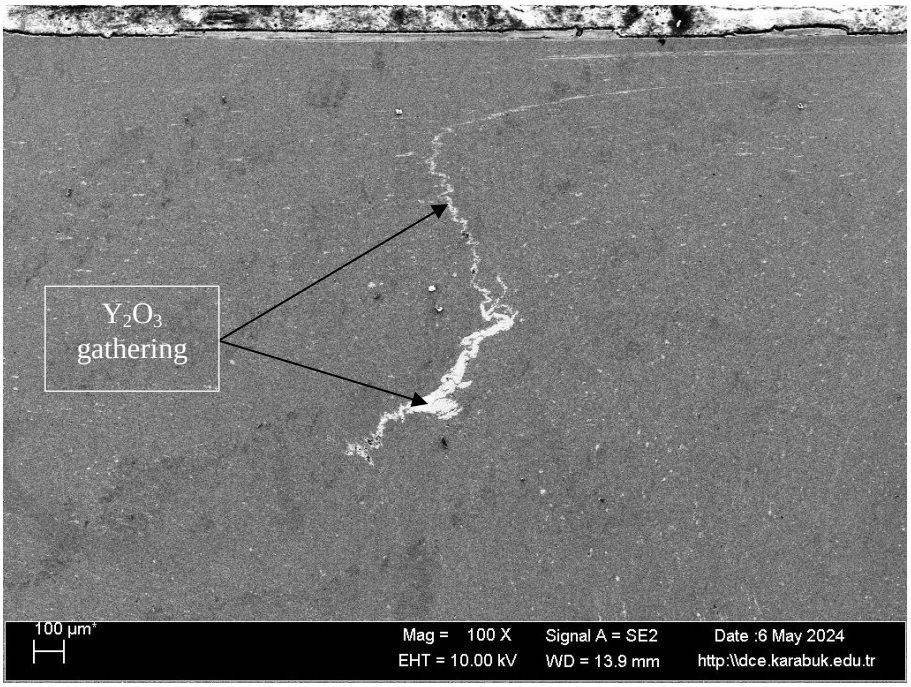

Figure 4.7. SEM images of samples no. 6

From above Figures 4.6 and 4.7, can see SEM images and how the distribution of the particles.

There is an accumulation of Y_2O_3 at the edge of the FZ as a result of its uneven distribution, which led to its concentration along the border between SZ and TMAZ, as Figure 4.7. shown.

4.1.3. Energy Dispersion Spectrometry Result

The examination using energy dispersion spectrometry (EDS) shows how the particles distribute in the layers of sample no. 9 shown in Figure 4.8. Where particles distributions percent is given in Table 4.1.

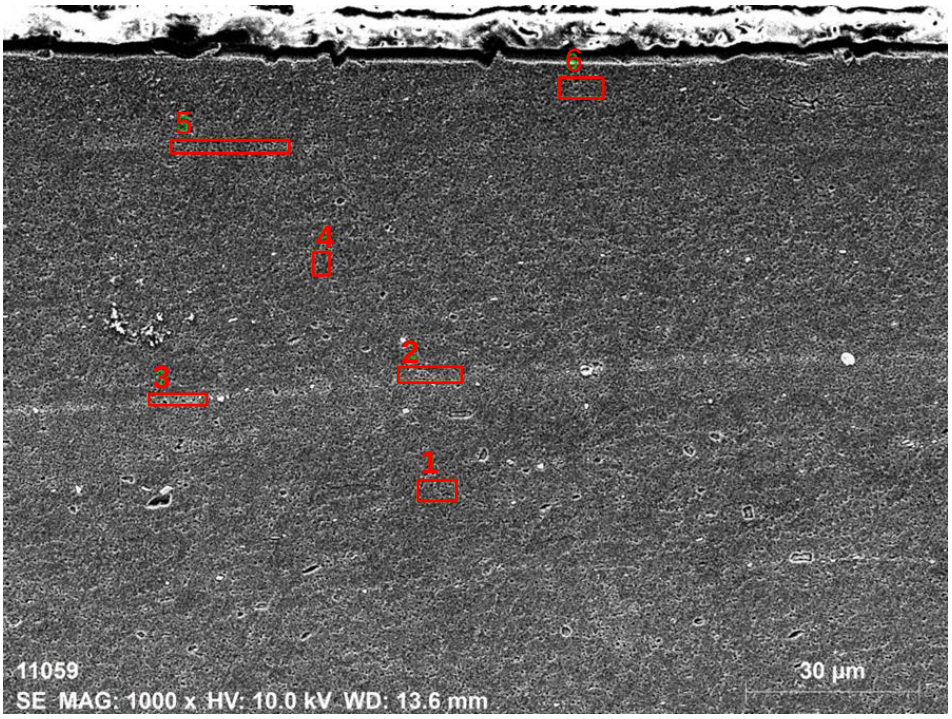

Figure 4.8. EDS analaysis for specimen no. 9 side surface

Table 4.1 EDS analysis elements details at pointed sites for specimen no. 9

Mass percent (%)

Spectrum	O	Mg	Al	Fe	Cu	Zn	Y
1	2.34	2.89	82.19	0.65	4.24	7.51	0.18
2	2.96	2.85	80.30	0.00	4.71	7.66	1.52
3	3.94	2.92	78.72	0.00	3.07	7.16	4.19
4	2.41	2.99	82.47	0.30	4.13	7.70	0.00
5	2.59	2.84	82.53	0.00	4.15	7.89	0.00
6	2.59	2.88	83.22	0.00	3.25	7.96	0.10
Mean value:	2.80	2.89	81.57	0.16	3.93	7.65	1.00
Sigma:	0.60	0.05	1.71	0.27	0.63	0.29	1.67
Sigma mean:	0.24	0.02	0.70	0.11	0.26	0.12	0.68

For EDS quantification of these features an accelerating voltage of 10 kV was used since this was sufficient to generate all elemental peaks of interest. To optimize the chemical analysis of Al, Zn, Cu, Mg, O, Y and Fe present in the sample, Figure 4.9. shows Al peak is much stronger than the compared to the other elements peaks [65].

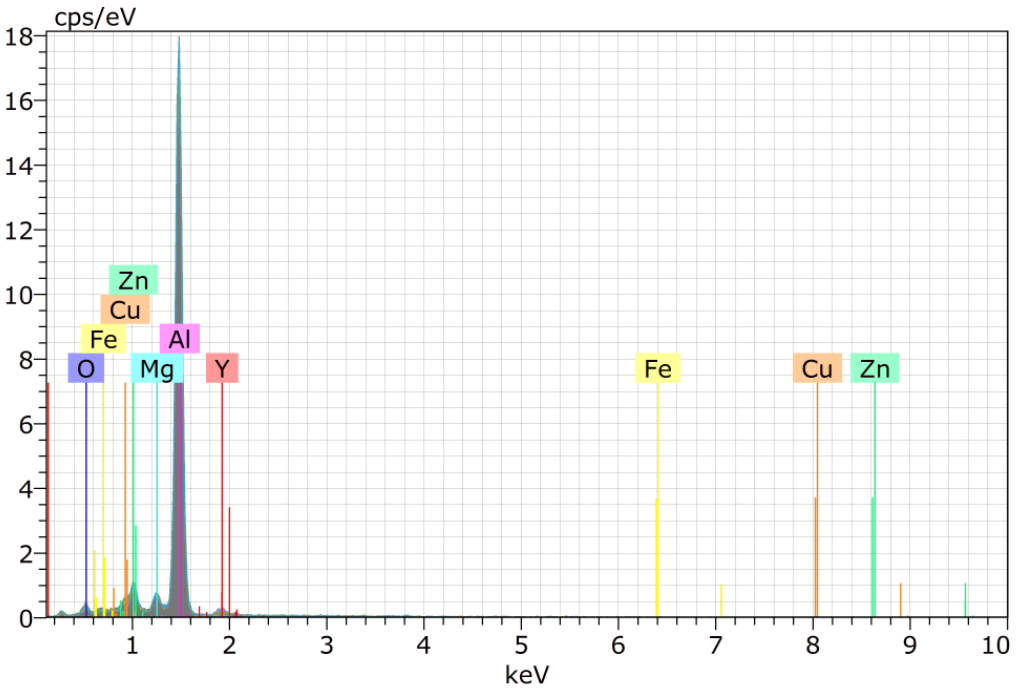

Figure 4.9. Elements peaks for the specimen no.9 side surface

From Figure 4.9 Aluminum peak is easily detectable where other elements peaks were lower than Aluminum peak, that's prove what was shown in OM and SEM images.

Figure 4.10 below we can see very clearly how the elements distributed in the layers and mixed with the Al particles, and how was the effect of the FSP on the base material.

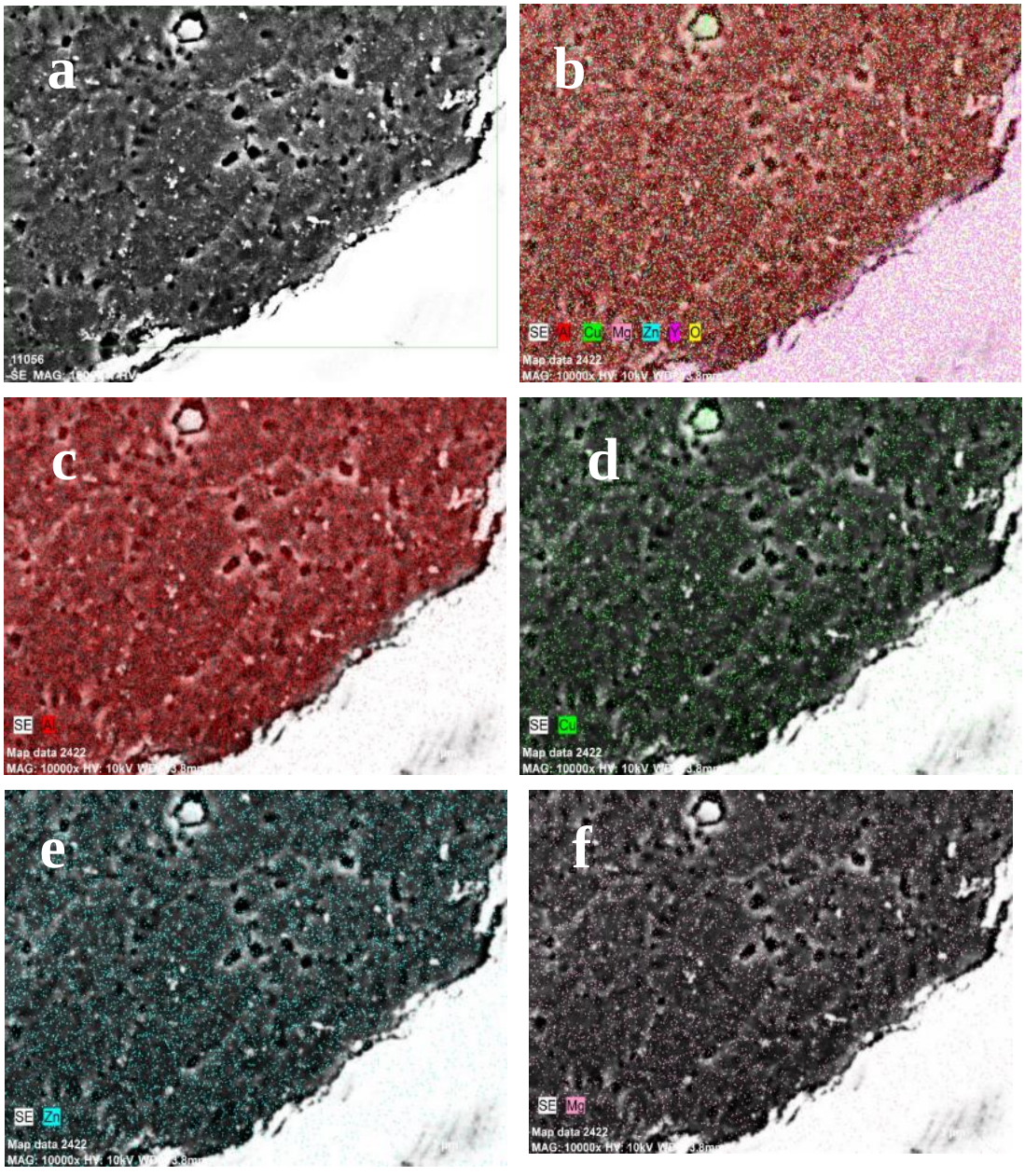

Figure 4.10 Continuous qualitative EDS mapping analysis elements details at pointed for the Specimen no. 6 (a) scan image (SE) (b) SE + Al, Zn, Cu, Mg, O, Y and Fe (c) SE + Al (d) SE + Cu (e) SE + Zn (f) SE + Mg

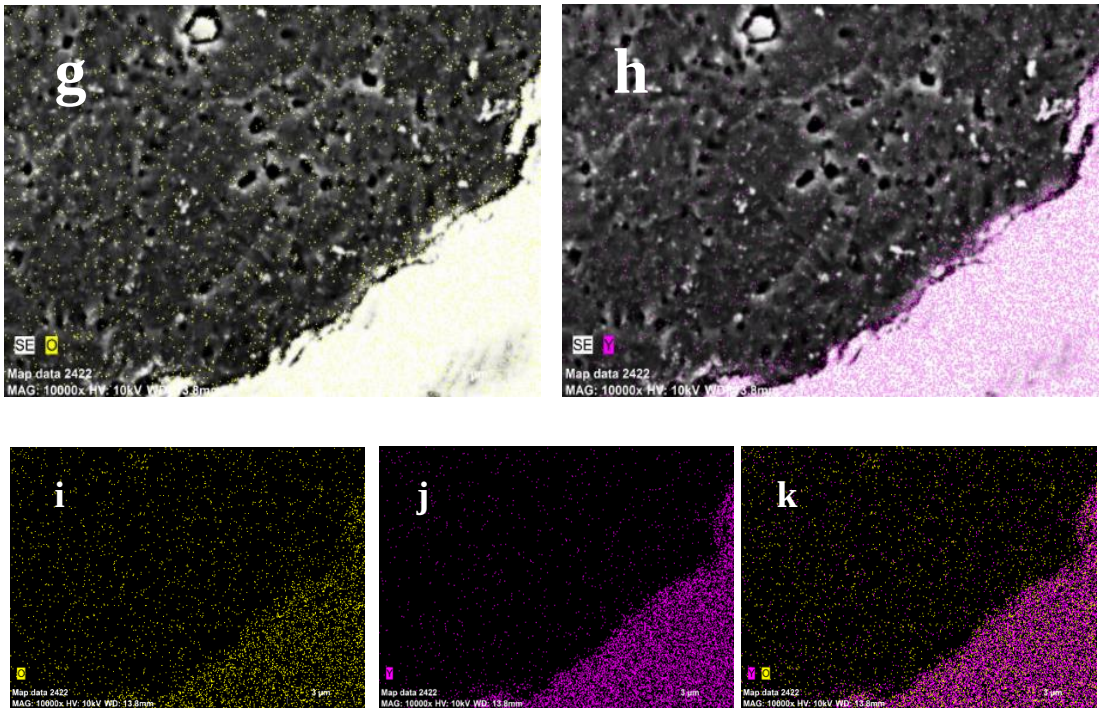

Figure 4.10. Continuous qualitative EDS mapping analysis elements details at pointed for the Specimen no. 6 (g) SE + O (h) SE+Y (i) O (j) Y (k) YO

Figure 4.10 shows the distributions of the elements, and we can notice the accumulation of the Y_2O_3 in the lower right side of the images due to the gathering of the non-powder because of up normal distributions of the Y_2O_3 particles for this area.

4.1.4. X-Ray Diffraction

X-ray diffraction (XRD) is a powerful tool used to identify the minor and major single or multiple phases present in an unknown sample. This technique is particularly useful in materials science and engineering, where understanding the composition and structure of materials is crucial for their proper functioning and application.

Figure 4.11 shows the XRD analysis of samples numbered 4, 9 and base material. As can be seen from the XRD of these three samples, similar phases formed in the samples and no significant change was observed. A part of the sample 9 XRD graph is enlarged to show the general phase distribution in more detail.

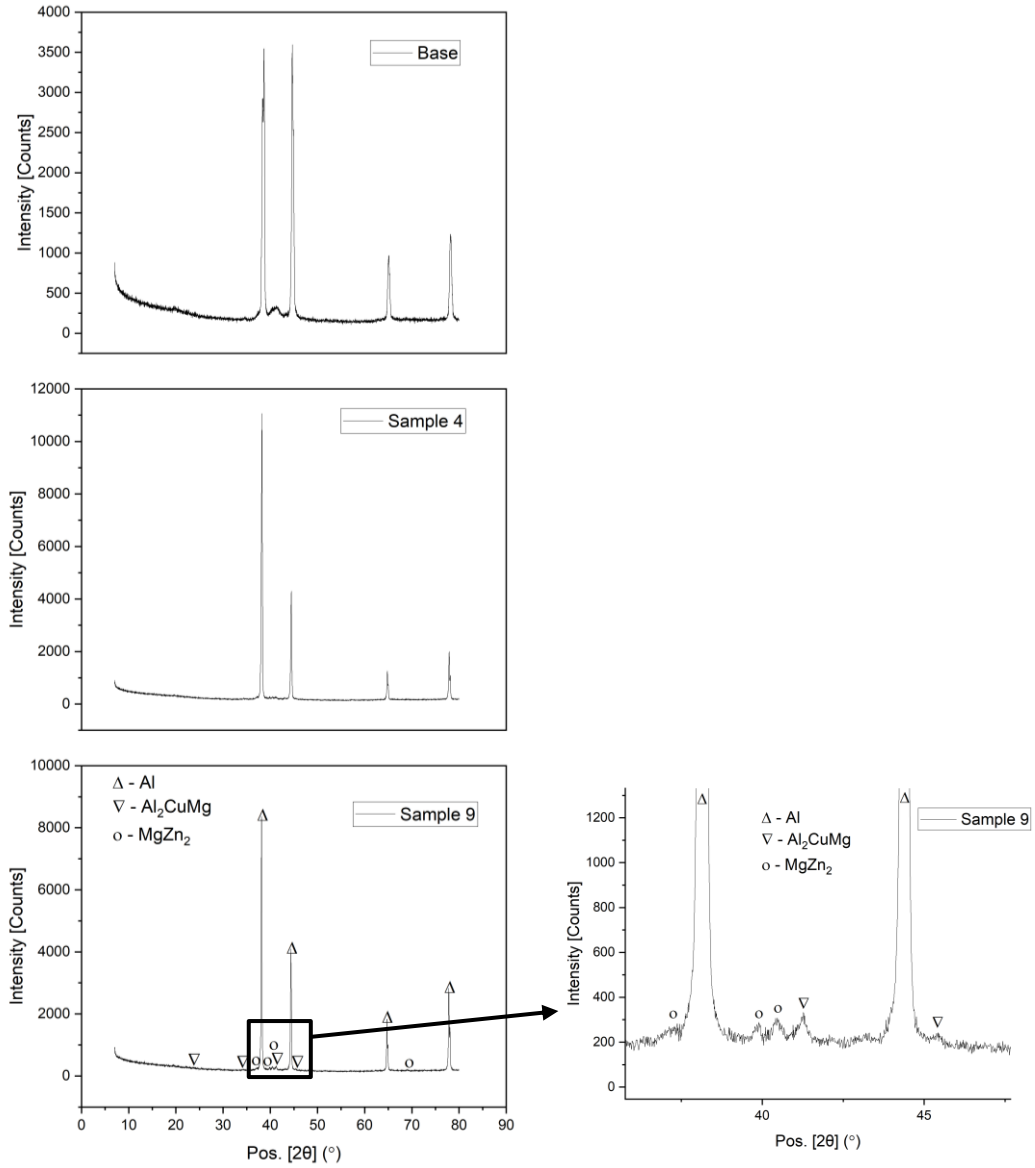

Figure 4.11. XRD pattern of specimen no. 9

Figure 4.11. shows the results of XRD which identified the phases of Aluminum, Magnesium, Copper, and Zinc from sample no. 9. It does not need much clarification and explanation because the base metal is the same and Y_2O_3 has been added, which is a nanomaterial that does not have a significant effect on the basic elements of the base material.

It shows peak of spik of Al and has a minor content of Al_2CuMg and $MgZn_2$ as a chemical component percentage from the base material chart in the Table 4.1.

4.2. MECHANICAL RESULT

4.2.1. Hardness Test Result

The widthwise microhardness profile of the stir zone, along with the average microhardness of the base material 7075-T73 aluminum, are shown in Table 4.2 for nineth processing conditions.

Table 4.2 Average hardness on the upper surface of specimens

Sample No.	Parameter		Average Hardness	
	Rotational speed	Travel speed	HV	
	rpm	mm/min	HAZ	TMAZ
1	710	55	118.03	128.6
2	710	70	120.06	150.95
3	710	90	146.63	139.95
4	900	55	110.96	124.6
5	900	70	134.06	130.45
6	900	90	142.9	143.4
7	1120	55	120.33	117.55
8	1120	70	140.8	133.1
9	1120	90	148.6	129.65
Base material	-	-	141.5	

The microhardness was measured at 4.9N on the upper surface of the SZ and TMAZ. The average microhardness of the base material 7075-T73 was 141.5 Hv. For the workpiece processed using a pin depth of 2.7 mm, the surface composite's microhardness was, remarkably, abnormal result of the presence of the reinforcement Y_2O_3 particles in the HAZ and TMAZ are shown in Figure 4.10. High hardness values, approaching 150 Hv, were recorded near the middle of the stir zone for the samples 710 rpm / 90 mm/min, 900 rpm / 90 mm/min and 1120 rpm / 90 mm/min, 146.7, 142.9 and 148.6 Hv respectively, which is consistent with the OM and EDS results, supporting the production of excellent Y_2O_3 dispersion in the thick composite layer at the center of the stir zone.

Beyond 4 mm from the center, a reduction in the hardness was shown to occur, reaching a minimum value of approximately 139.9 and 129.6 Hv 710 rpm / 90 mm/min and 1120 rpm / 90 mm/min, respectively. The composite/matrix interface, which is lower than the hardness recorded for the base material 141.5 Hv only 900 rpm / 90 mm/min which was recorded 142.9 Hv.

The reduction in hardness demonstrates that the dispersion of Y_2O_3 particles into the base material became less effective as the distance from the tool center increases.

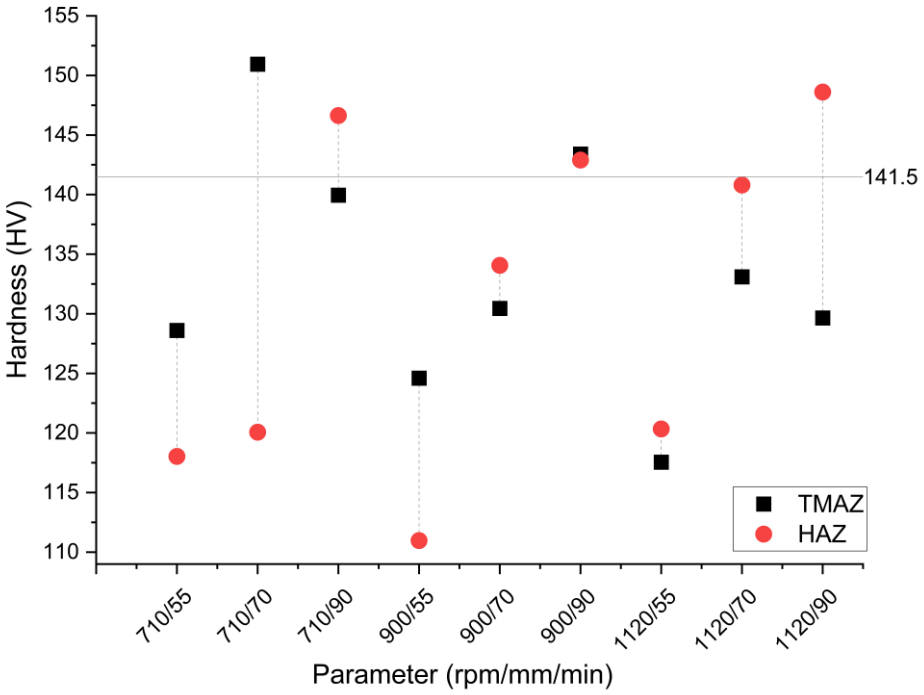

Figure 4.12. Vickers test graph for upper surface TMAZ, HAZ

Figure 4.12 and Table 4.2 can see that the microhardness decreased with travel speed (55 mm/min), while the Vickers hardness increased with travel speed (90 mm/min).

Where several tests were taken for microhardness of the upper surface, including 5 points for all samples, 2 for the middle area and 3 for the right for all specimens and take the average hardness for each area, while 30 tests surface were taken of samples no. 3, 6, and 9, five points were test on the right, 5 on the left, and 30 in the middle area, and take the average hardness for each area.

The Vickers microhardness profile of a horizontal line at the upper surface of the samples shown in the table and Figure 4.13.

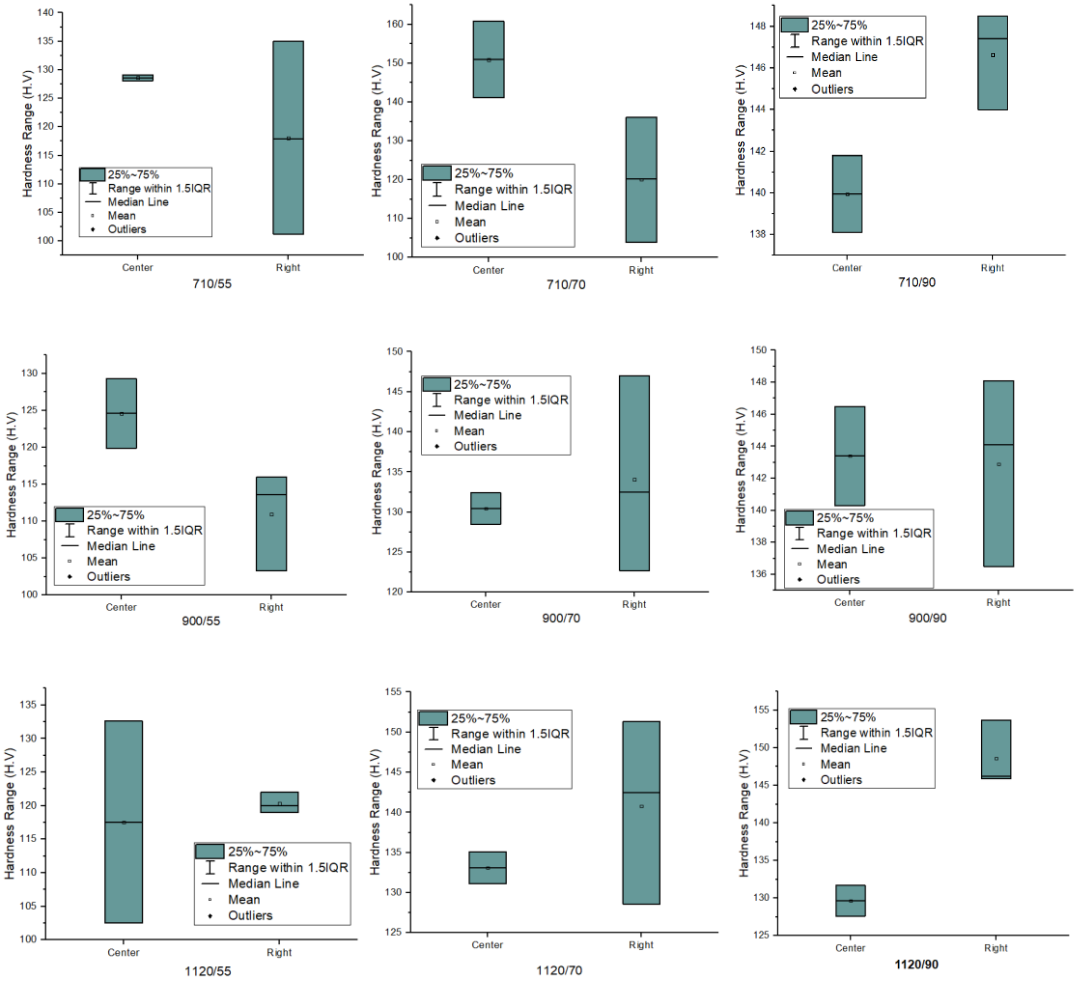

Figure 4.13. Microhardness profile of a horizontal line at the upper surface

Microhardness indentations were measured at 4.9N for the side surface of SZ and TMAZ of the specimens. The average microhardness of the base material aluminum 7075-T73 was 158 Hv shown in Table 4.3.

Table 4.3 Hardness test for side surface of specimens

Sample No.	Parameter		Average hardness		
	Rotational speed rpm	Travel speed mm/min	HV		
			Left	Centre	Right
1	710	55	97	104	110
2	710	70	113	121	121
3	710	90	105	112	101
4	900	55	122	121	124
5	900	70	101	99	104
6	900	90	109	124	121
7	1120	55	119	127	124
8	1120	70	118	125	126
9	1120	90	126	129	130
Base material	-	-		158	

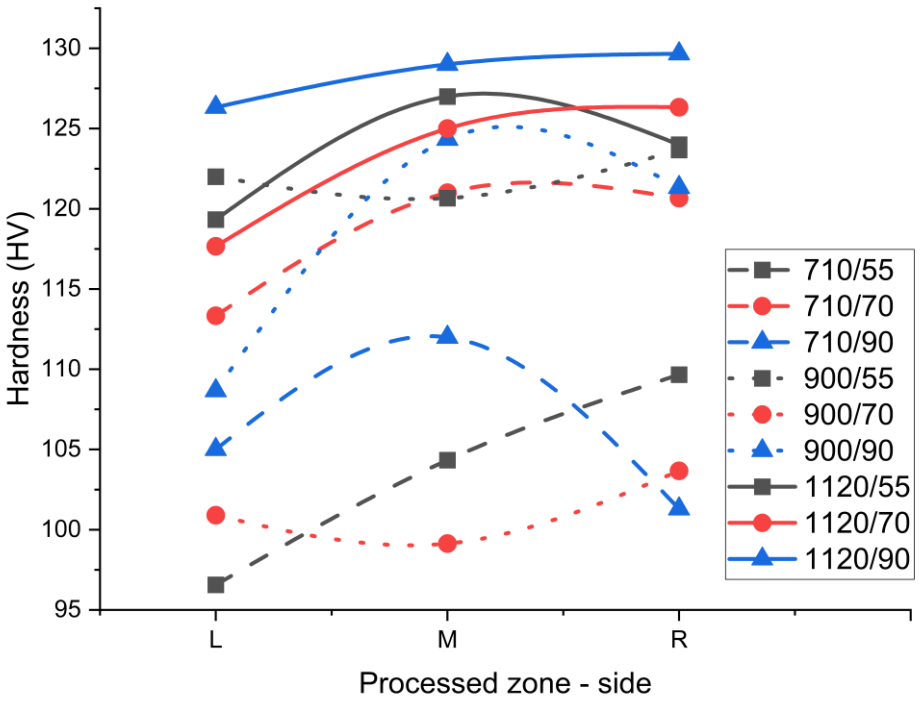

Figure 4.14. Vickers test graph for side surface SZ, TMAZ

Figure 4.14 and Table 4.3 can see that the microhardness gave lower average value when the Rotational speed in (710, 900 rpm) and the travel speed (55, 70 mm/min) while the highest value for the 1120 rpm and 90 mm/min in average, but still lower than the base material.

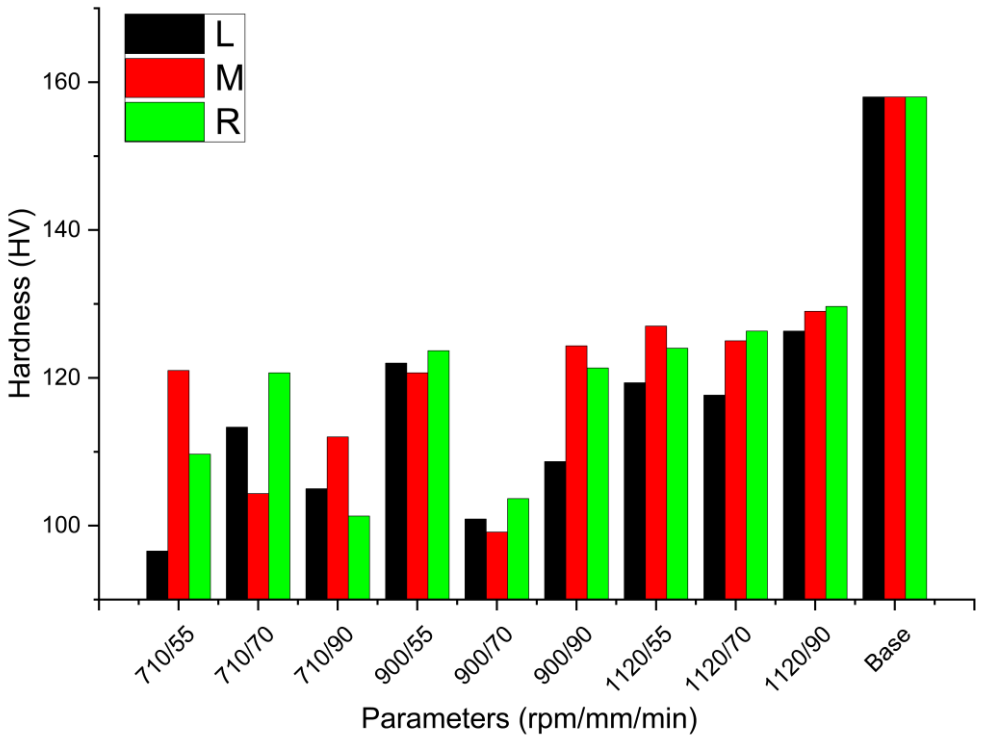

Figure 4.15. Vickers hardness from side surface of samples

In general, the rotational speed of 1120 rpm gave the best values of all travel speeds as Figure 4.15. Vickers test column graph for side surface. The effect of heat as a result of the process is evident on the annealed metal. The hardness of the metal used (Al 7075-T73) is about 155 Hv, while the hardness of the metal Al 7075 without heat treatment does not exceed 68 Hv.

4.2.2. Tensile Test Result

The test of tensile of the specimens Figure 4.16 were made to see the behaver of the Al 7075 -T73 after different parameters, as shown in the Table 4.4.

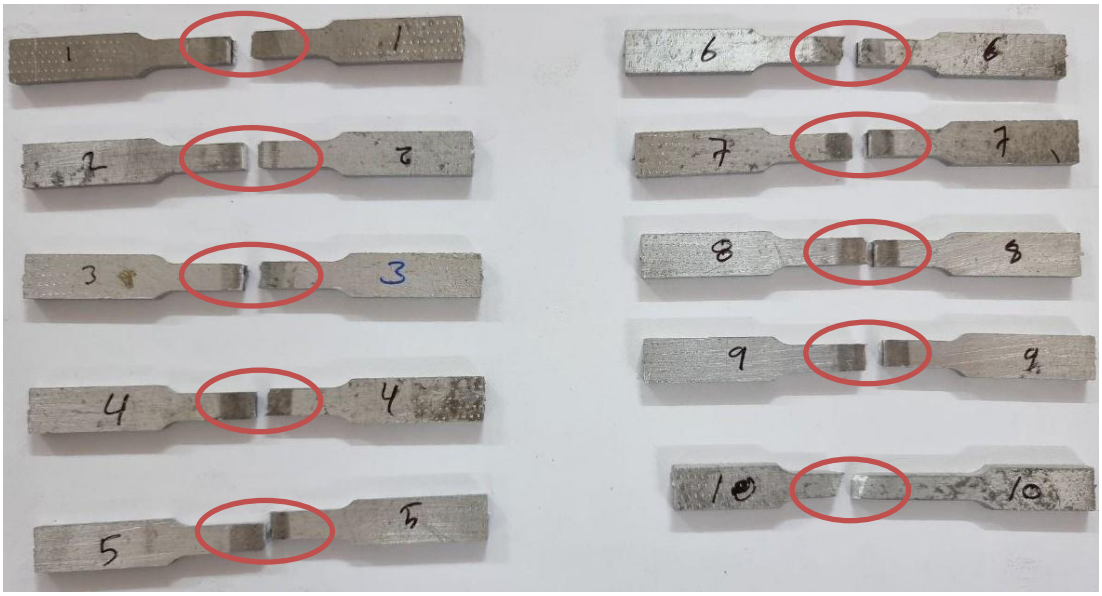

Figure 4.16. Tensile specimens after the test

Tensile test results are given in Table 4.4.

Table 4.1 Tensile strength for the specimens

Sample No.	Rotational Speed (rpm)	Travel Speed (mm/min)	Yield Strength (MPa)	Ultimate Tensile Strength (MPa)	Relative Ultimate Tensile Strength (%)	Elongation (%)
1	710	55	406	407	77	1.492
2	710	70	88	157	30	0.803
3	710	90	281	281	53	0.929
4	900	55	304	362	69	1.405
5	900	70	394	394	75	1.297
6	900	90	348	352	67	1.145
7	1120	55	281	290	55	1.083
8	1120	70	336	384	73	1.376
9	1120	90	343	363	69	1.192
Base mat.	-	-	290	525.4	100	13

From the above Table 4.4 that shows highest value of YS, UTS and elongation for specimen no. 1 which has a lower rotational and travel speed (710/55) while

specimen no. 2 gives lower value (710/70) (406,407 and 1.192%), (88,175, 0.803%) respectively, and specimen no. 3 (710/90) has (281, 281, and 0.929%) value.

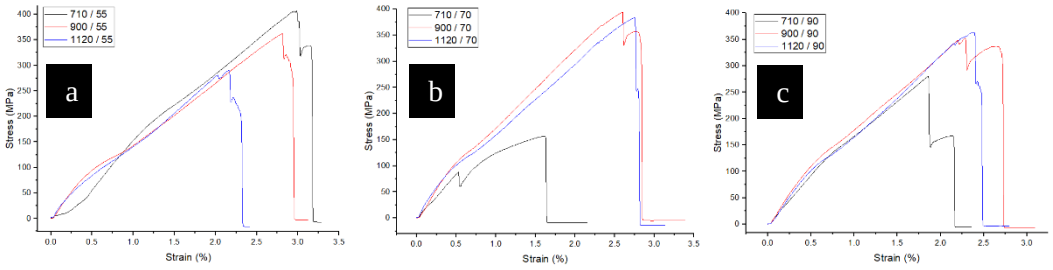

Figure 4.17. The tensile graphs of three travel speed groups (a) (710, 900, 1120) / 55 - (b) (710, 900, 1120) / 70 - (c) (1120, 900, 1120) / 55

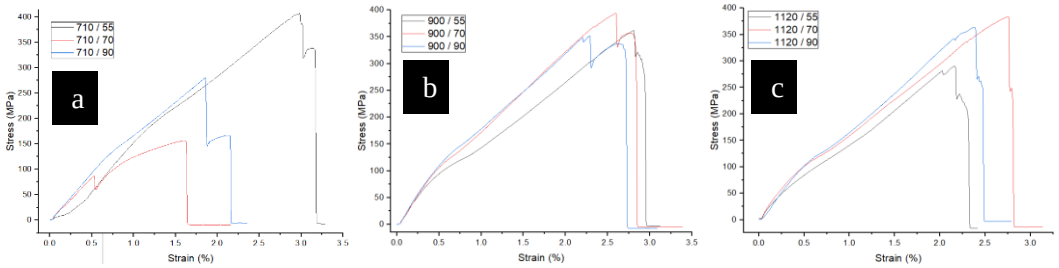

Figure 4.18. The tensile graphs of three rotational speed groups (a) 710 / (55,70,90) - (b) 900 / (55,70,90) - (c) (1120 / 55,70,90)

If we look from different side can see the second-best value goes to the specimen no. 9 (1120 rpm /90 mm/min) for the high rotational and travel speed (YS:343, UTS:363 and E% 1.19) and the specimen No.6 (900 rpm /90 mm/min) has a close value to the specimen no. 9 (YS:348, UTS:352 and E% 1.145).

This proves that the decrease in the tensile value is due to the tunnel that resulted from the FSP process for all samples except specimens no. 1 (710 rpm /55 mm/min) and no. 9 (1120 rpm /90 mm/min).

Table 4.2 Mechanical properties of Al 7075 and 7075-T73

Material		Yield Strength MPa	Tensile Strength MPa	Elongation %	Hardness Hv
AA7075	Standard	103	228	10	68
AA7075-T73	Standard	435	505	13	155
AA7075-T73	Measured	290	525	13	158

In fact, the tensile strength of the FS processed Al 7075-T73 is lower than of the base material due to the heat generated during the process, which affects the mechanical properties and microstructure [66].

From Figure 4.19 can see the behaver of all specimens and how different the results.

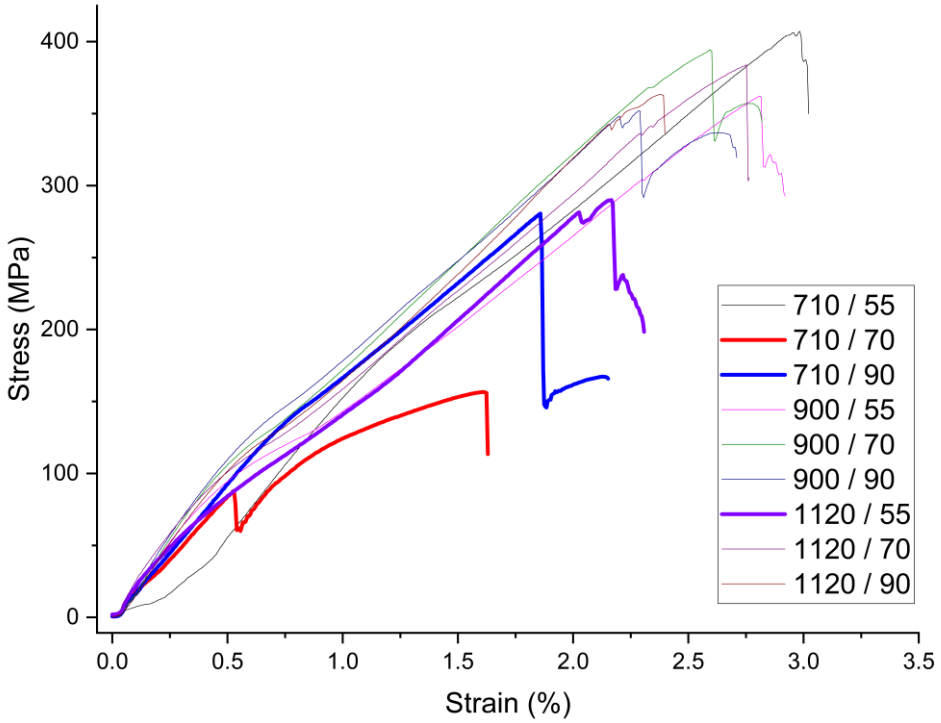

Figure 4.19. The tensile graph of specimens

The correlation between tensile strength and hardness is nonlinear, with the tensile strength being lower than expected at higher hardness values. This is evident from the slight underprediction of tensile strength at higher hardness values [67].

4.2.3. Bending Test Result

The bending test was made to see the behaver of the Al 7075 -T73 after different parameters. In this test three-point bending, the distance between the 2 supporting pins was 80 mm, whereupon diameter 30 mm. as Figure 4.20 shows, while the test results given in the Table 4.6.

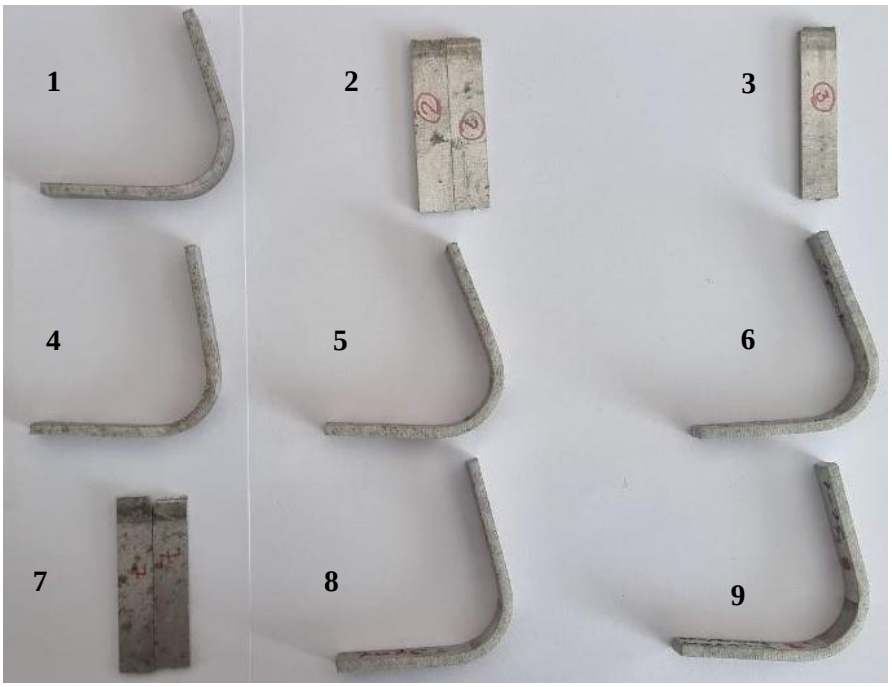

Figure 4.20. Specimens after bend test

Table 4.3 Bend strength of specimens

Sample No.	Rotational Speed (rpm)	Travel speed (mm/min)	Yield stress (MPa)	Bending angle (degree)
1	710	55	7.15	66.57
2	710	70	4.85	26.48
3	710	90	5.05	29.53
4	900	55	6.85	64.52
5	900	70	6.85	65.16
6	900	90	6.75	67.05
7	1120	55	2.75	07.21
8	1120	70	7.20	65.97
9	1120	90	7	66.62

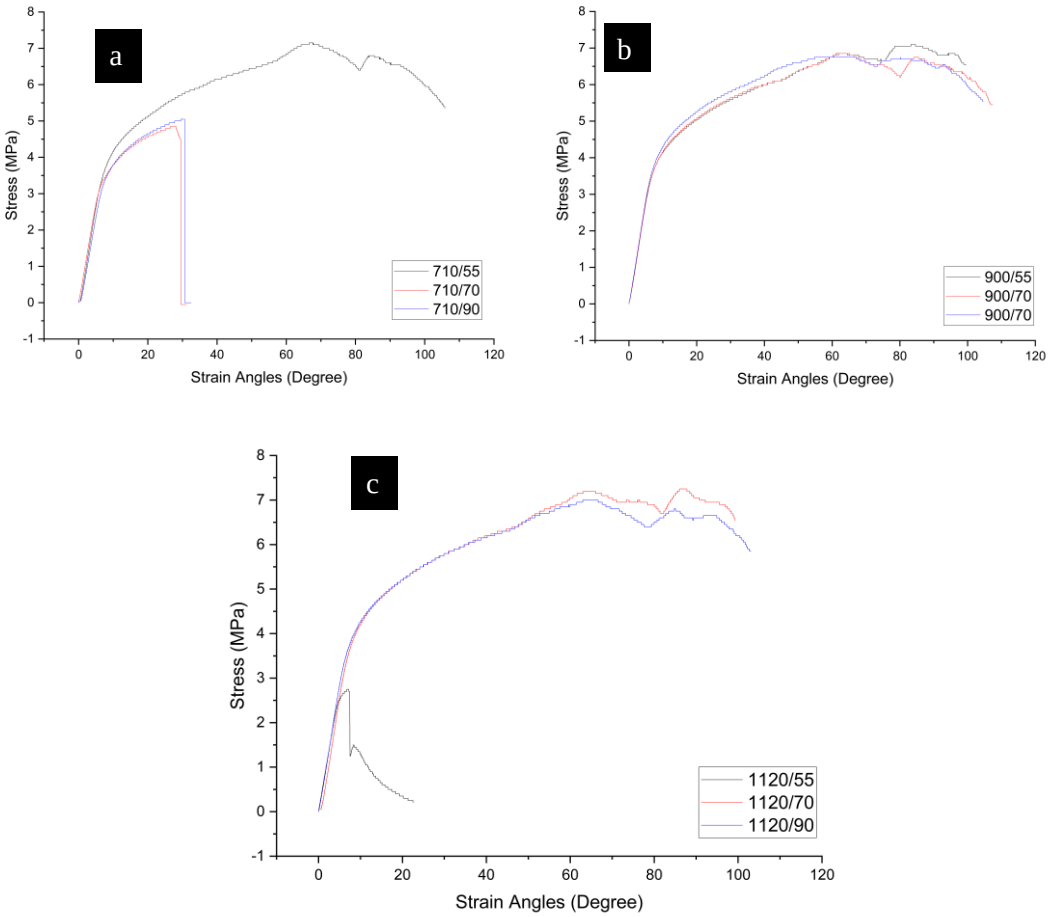

Figure 4.21. Bend graphs of three rotational speeds groups (a) 710 / 55,70,90 - (b) 900 / 55,70,90 - (c) 1120 / 55,70,90

From the above Figure 4.21. (a, b and c) three of nine specimens failed during the bending test at 5.05 MPa or less and maximum 30 degrees of bend, where the specimens 1120 rpm /55 mm/min has 7.21 bend angle degree at 2.75 MPa stress and the specimens 710 rpm /70 mm/min and 710 rpm /90 mm/min has 26.48 29.53 angle bend degree and 4.85, 5.05 MPa stress respectively, while all other specimens passed the tests successfully.

The specimens with 900 rpm / (55, 70 and 90 mm/min) have a closet value with (6.85, 6.85 and 6.75) angle bend degree at (64.52, 65.16, 67.05) MPa stress respectively. Where the specimens 1120 rpm /70 mm/min get best value 65.97 bend angle degree at 7.20 MPa stress and the specimens 710 rpm /55 mm/min get 66.57 bend angle degree at 7.15 MPa stress while the specimen 1120 rpm /90 mm/min get 66.62 bend angle degree at 7 MPa stress.

4.2.4. Wear Test Result

Wear apparatus, with a speed of 950 rpm, 10N load, distance from disk center 6.5cm, (5, 10, 15) minutes at room temperature . Figure 4.22 shows the wear specimens after the test.

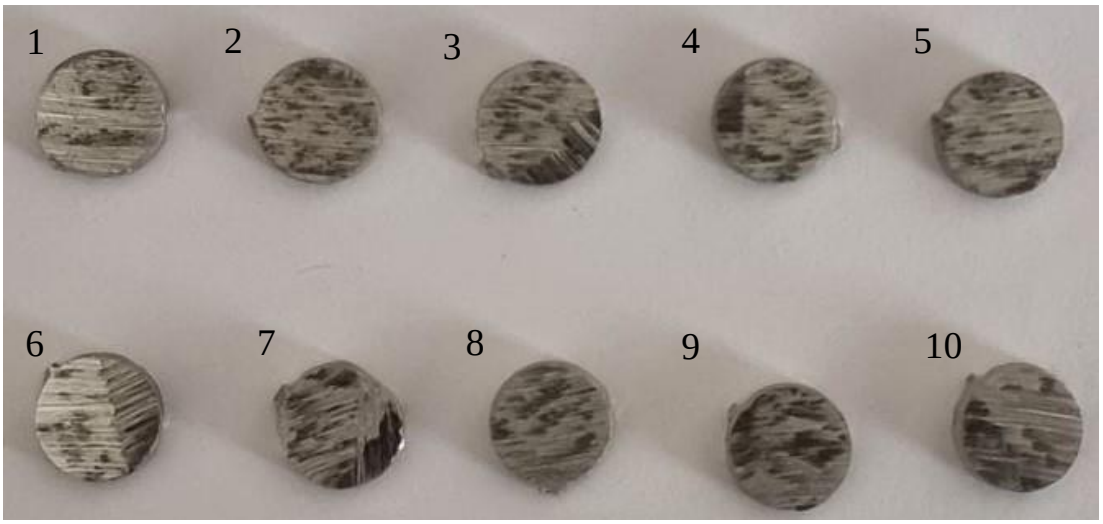

Figure 4.22 Specimens after wear test

Wear tests results shown in the Table 4,7 and 4.8, where we can see that the Sample no. 1 (710 rpm /55 mm/min) has the loest loss of weight among other samples record 0.0087 g after 15 min, then comes sample no. 4 (900 rpm /55 mm/min) has 0.0100 g in weight loss, where the samples no. 5 (900 rpm /70 mm/min) and no. 8 (1120 rpm /70 mm/min) recorded a close loss in weight 0.0105, 0.0108 respectively, while the Sample no. 6 (900 rpm /90 mm/min) recorded highest loss in weight, about 0.0141 g, in the other hand the samples no. 3 (710 rpm /90 mm/min) and no. 9 (1120 rpm /90 mm/min) shows a close loss in weight 0.0111, 0.0117 respectively, Moreover, the samples no. 2 (710 rpm /70 mm/min) and no. 7 (1120 rpm /55 mm/min) recorded a close loss in weight 0.0121, 0.0123 respectively.

Table 4.4 Specimens weights after 5, 10, 15 minutes due to wear test

Sample No.		W_1	W_2	W_3	W_4
		0	**5**	**10**	**15**
1	710/55	0.6382	0.636	0.6324	0.6295
2	710/70	0.6221	0.6209	0.6167	0.61
3	710/90	0.6193	0.6182	0.6152	0.6082
4	900/55	0.6132	0.6123	0.609	0.6032
5	900/70	0.6248	0.6226	0.6185	0.6143
6	900/90	0.6359	0.6336	0.6289	0.6218
7	1120/55	0.6194	0.618	0.6147	0.6071
8	1120/70	0.617	0.6147	0.6114	0.6062
9	1120/90	0.6256	0.6236	0.6177	0.6139
10	Base material	0.6634	0.6611	0.6581	0.6531

Table 4.5 Loss of weight (g) after 5, 10 and 15 minutes

Sample No.		Time / min		
		5	**10**	**15**
1	710/55	0.0022	0.0058	0.0087
2	710/70	0.0012	0.0054	0.0121
3	710/90	0.0011	0.0041	0.0111
4	900/55	0.0009	0.0042	0.01
5	900/70	0.0022	0.0063	0.0105
6	900/90	0.0023	0.007	0.0141
7	1120/55	0.0014	0.0047	0.0123
8	1120/70	0.0023	0.0056	0.0108
9	1120/90	0.002	0.0079	0.0117
10	Base material	0.0023	0.0053	0.0103

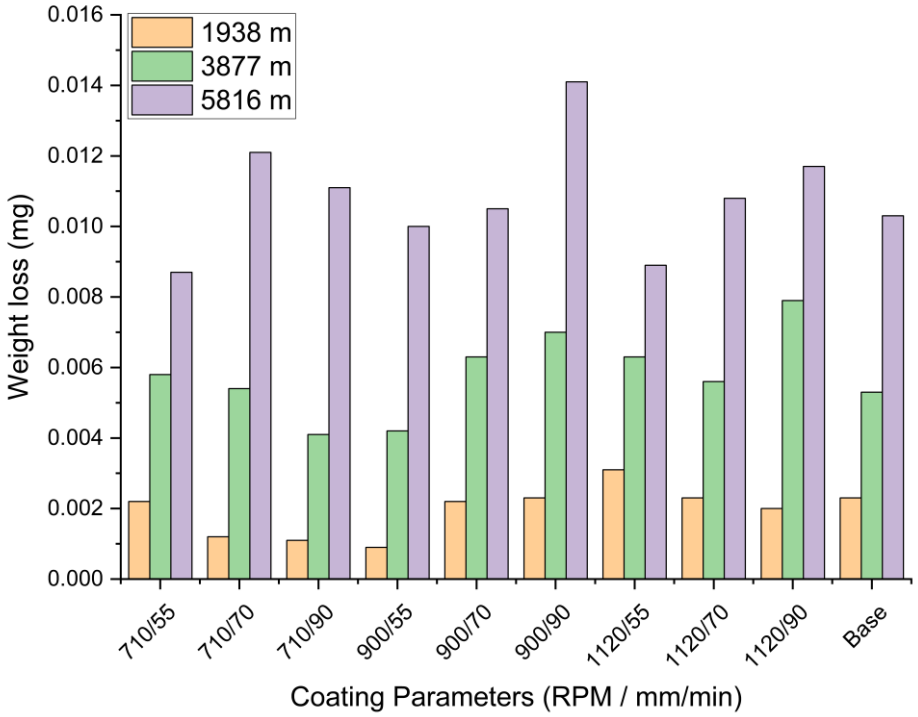

Figure 4.23. The weight loss after wear test graph

The OM image of Aluminum 7075-T73 was shown in Figure 4.24. It shows the worn surfaces of the base material.

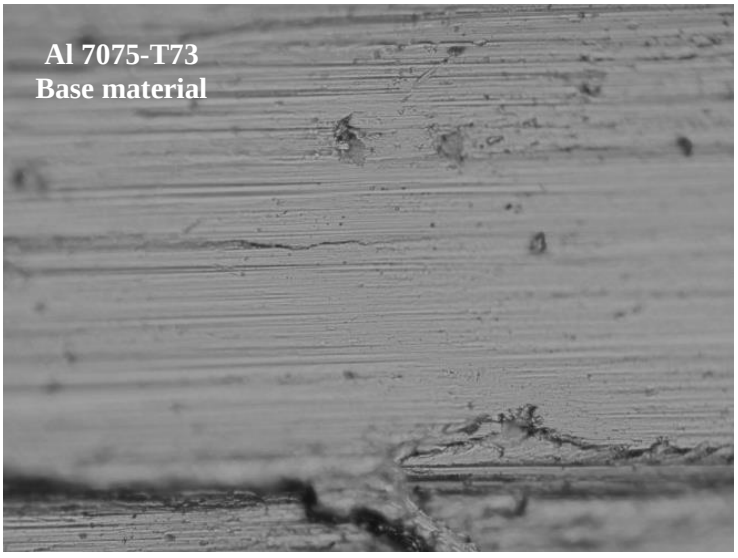

Figure 4.24. The worn surface of base material (Al 7075-T73)

Figure 4.24 exhibit finer grooves and slight plastic deformation at the edges of the grooves, the surface also appears to be smooth of base material specimen.

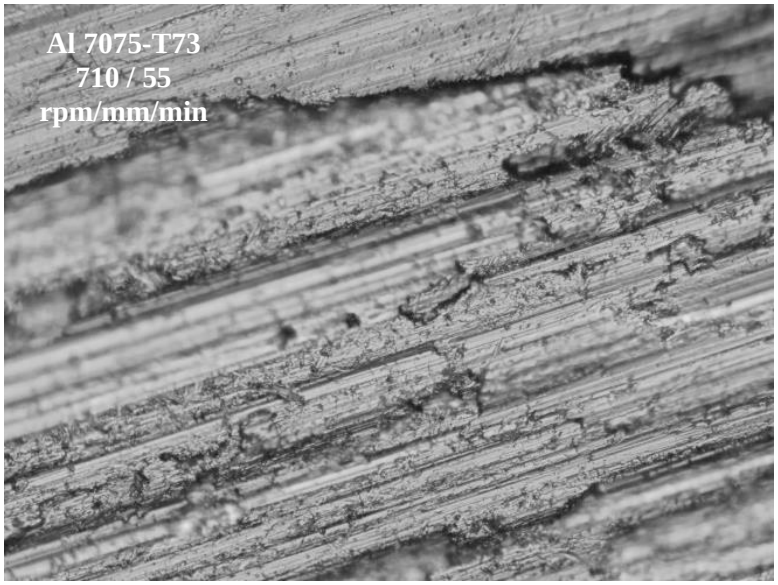

Figure 4.25. The worn surface of specimen no. 1

Figure 4.25 above exhibits greater grooves and significant plastic deformation at the edges of the grooves of specimen no. 1, the surface appears to be rough because of the Y_2O_3 reinforcement content.

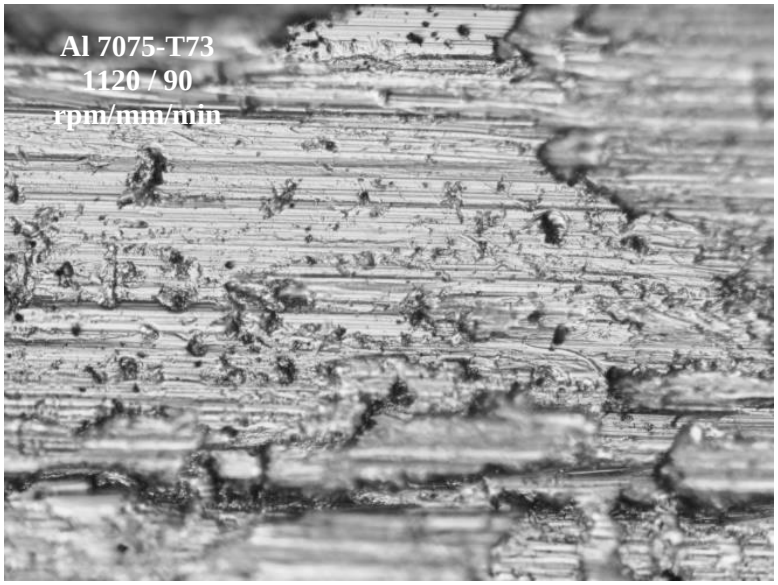

Figure 4.26. The worn surface of specimen no. 9

From the above Figure 4.26 exhibits fine grooves and middle plastic deformation at the edges of the grooves of specimen no. 9, the surface appears to be rough because of the Y_2O_3 reinforcement content.

Wear Rate

The specific wear rate S.W.R calculated from equation below [68].

$S.W.R=\Delta m/ (\rho \times p \times x)$

Where:

Δm : average mass loss (g),

x : sliding distance (mm),

p : applied load (N)

ρ : density of the materials (g mm)

Total sliding distance x was calculated as follows

$x= 2 \pi \times D \times n \times t$

Where:

D : distance from the center of sample to the center of disc in meter

N : linear sliding speed (mm/min)

T : time of running (15 min)

Where:

Disc Radius: 6.5 cm = 0.065 m,

Disc Speed: 950 RPM,

Normal Load: 10 N

Table 4.6 The wear rate for 5, 10, 15 minutes due to wear test

Sample No.		Time / min		
		5	10	15
1	710/55	2.94	3.88	3.88
2	710/70	1.60	3.61	5.40
3	710/90	1.47	2.74	4.95
4	900/55	1.2	2.81	4.46
5	900/70	2.94	4.21	4.60
6	900/90	3.08	4.68	6.29
7	1120/55	4.15	4.21	3.97
8	1120/70	3.08	3.75	4.82
9	1120/90	2.67	5.29	5.22
10	Base material	3.08	3.54	4.59

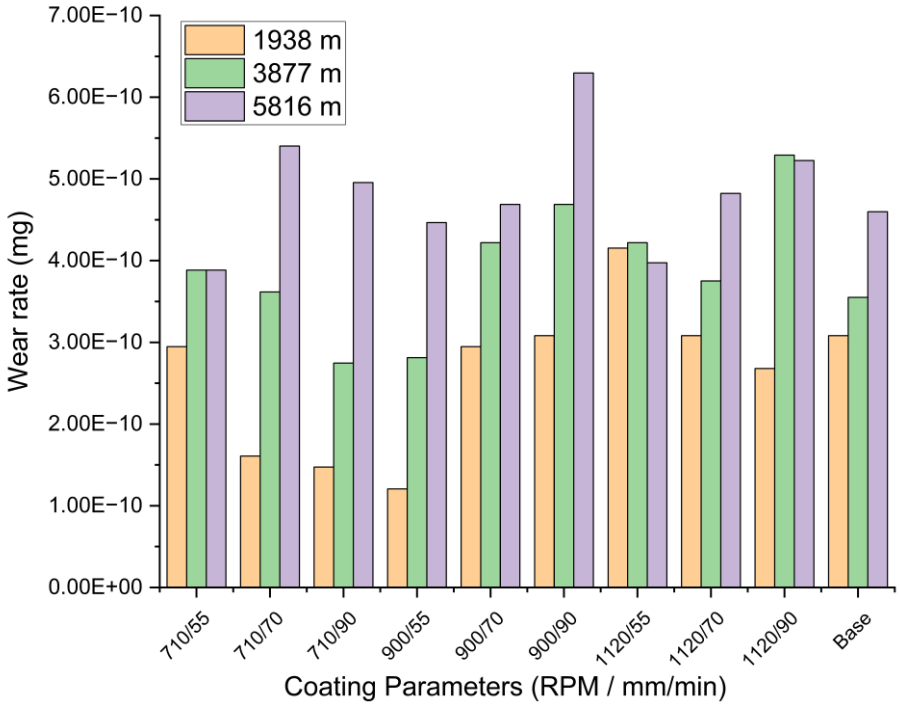

Figure 4.27. The wear rate graph

From the above Table 4.9 and Figure 4.27 can see the wear rate at the first at 5 minutes the specimen 900 rpm / 55 mm/min has a lower wear rate 1.2 then 1.47 for the specimen 710 rpm / 90 mm/min and 710 rpm / 70 mm/min with 1.6 wear rate while the base material, and specimens 900 rpm / 90 mm/min, 1120 rpm / 55 mm/min had 3.08 wear rate but the specimen 1120 rpm / 55 mm/min has a highest wear rate 4.15.

But after 15 minutes the wear rate totally changed, so the specimen 900 rpm / 90 mm/min has a highest wear rate 6.29 then 5.4 and 5.22 for the specimens 710 rpm / 70 mm/min, 1120 rpm / 90 mm/min respectively, the optimum wear rate gotten 3.88 from specimen 710 rpm / 55 mm/min. Which was maintained during the three examination times. The reason is due to the homogeneous distribution of particles, and the absence of gaps and tunnels.

PART 5

CONCLUSIONS AND RECOMMENDATIONS

This research's primary goal was to enhance the surface properties of aluminum alloys 7075-T73 using friction stir processing (FSP) and study the microstructure and mechanical properties of the aluminum alloys 7075-T73 after process.

5.1 CONCLUSIONS

1. In the process of aluminum alloys 7075-T73, a specimen with a rotational speed of 710 rpm and a travel speed of 55 mm/min and a specimen with a rotational speed of 1120 rpm and a travel speed of 55 mm/min were selected as the optimum specimens due to their wear rate.
2. The microhardness decreased with travel speed 55 mm/min, while the microhardness increased with travel speed 90 mm/min specimen with a rotational speed of 1120 rpm, and a travel speed 90 mm/min were selected as the optimum specimens due to their hardness value.
3. The highest value of yield strength 407 MPa obtained under the processing conditions was associated with the specimen with the rotational speed, travel speed, and elongation percentage of 710 rpm, 55 mm/min, and 1.4%, respectively.
4. Optical micrographs show tunnels in some specimens along the stir zone edge and gathering of Y_2O_3.
5. SEM-EDS elemental analysis indicates good mixing in the stir zone sufficient diffusion of Al 7075-T73 elements.
6. The stir zone produced finer grain compared to the base material.

5.2 RECOMMENDATIONS

1. Using the tool steel KS SKH 51in FSP / FSW for Al 70750- T73.
2. Increase travel and rotational speed by using Y_2O_3 micro-size particles.
3. Study the corrosion effects on Al 70750-T73 reinforced with Y_2O_3.

REFERENCES

1. J. Victor Christy, A. H. Ismail Mourad, M. M. Sherif, and B. Shivamurthy, “Review of recent trends in friction stir welding process of aluminum alloys and aluminum metal matrix composites,” Transactions of Nonferrous Metals Society of China (English Edition), vol. 31, no. 11, pp. 3281–3309, 2021, doi: 10.1016/S1003-6326(21)65730-8.

2. R. S. Mishra, Z. Y. Ma, and I. Charit, “Friction stir processing: a novel technique for fabrication of surface composite.” [Online]. Available: www.elsevier.com/locate/msea

3. M. Ákos, Á. Meilinger, and I. Török, “The importance of friction stir welding tool,” 2013. [Online]. Available: https://www.researchgate.net/publication/308054542

4. S. Wadekar, R. Soladhra, H. Barkade, and N. Thombare, “A Review on Friction Stir Technology,” Ijritcc, vol. 5, no. 6, pp. 1542–1549, 2017.

5. V. Sharma, U. Prakash, and B. V. M. Kumar, “Surface composites by friction stir processing: A review,” J Mater Process Technol, vol. 224, pp. 117–134, 2015, doi: 10.1016/j.jmatprotec.2015.04.019.

6. M. Y. Khalid, R. Umer, and K. A. Khan, “Review of recent trends and developments in aluminium 7075 alloy and its metal matrix composites (MMCs) for aircraft applications,” Results in Engineering, vol. 20, no. August, p. 101372, 2023, doi: 10.1016/j.rineng.2023.101372.

7. “https://www.xometry.com/resources/materials/7075-aluminum-alloy/”.

8. S. S. Li et al., “Development and applications of aluminum alloys for aerospace industry,” Journal of Materials Research and Technology, vol. 27. Elsevier Editora Ltda, pp. 944–983, Nov. 01, 2023. doi: 10.1016/j.jmrt.2023.09.274.

9. “https://live-aerospace-specification-metals.pantheonsite.io/aluminum-distributor/”.

10. P. Zhang, X. Yue, Y. Sun, H. Zhou, J. Zhang, and Y. Wang, “Research on the mechanism of microbial corrosion in the subsurface layer of 7075 aluminum alloy under different corrosion environments with ultra low temperature double increase effect,” Vacuum, vol. 227, Sep. 2024, doi: 10.1016/j.vacuum.2024.113348.

11. “https://asm.matweb.com/search/SpecificMaterial.asp?bassnum=ma7075t73/”.

12. M. Y. Khalid, R. Umer, and K. A. Khan, “Review of recent trends and developments in aluminium 7075 alloy and its metal matrix composites (MMCs) for aircraft applications,” Results in Engineering, vol. 20, no. August, p. 101372, 2023, doi: 10.1016/j.rineng.2023.101372.

13. B. Zhou, B. Liu, and S. Zhang, “The advancement of 7xxx series aluminum alloys for aircraft structures: A review,” Metals (Basel), vol. 11, no. 5, May 2021, doi: 10.3390/met11050718.

14. “https://www.matweb.com/search/DataSheet.aspx?MatGUID=6653b72914864cc0a0ff7adf5b720167/”.

15. W. H. Hunt, “Metal Matrix Composites,” Comprehensive Composite Materials, pp. 57–66, 2000, doi: 10.1016/B0-08-042993-9/00134-0.

16. R. Casati and M. Vedani, “Metal matrix composites reinforced by Nano-Particles—A review,” Metals (Basel), vol. 4, no. 1, pp. 65–83, 2014, doi: 10.3390/met4010065.

17. M. Imran and A. R. A. Khan, “Characterization of Al-7075 metal matrix composites: A review,” Journal of Materials Research and Technology, vol. 8, no. 3, pp. 3347–3356, 2019, doi: 10.1016/j.jmrt.2017.10.012.

18. “https://refractiveindex.info/?book=Y_2O_3&page=Nigara&shelf=main/”.

19. P. Singh and H. R. Kandikonda, “Friction stir processing of aluminum alloys,” 2021.

20. K. Chiteka, “Friction Stir Welding/Processing Tool Materials and Selection.” [Online]. Available: https://www.researchgate.net/publication/258332026.

21. R. Rai, A. De, H. K. D. H. Bhadeshia, and T. DebRoy, “Review: Friction stir welding tools,” Science and Technology of Welding and Joining, vol. 16, no. 4, pp. 325–342, May 2011, doi: 10.1179/1362171811Y.0000000023.

22. M. Ákos, Á. Meilinger, and I. Török, “The importance of friction stir welding tool,” 2013. [Online]. Available: https://www.researchgate.net/publication/308054542.

23. N. Gangil et al., “Fabrication of magnesium-nitip composites via friction stir processing: Effect of tool profile,” Metals (Basel), vol. 10, no. 11, pp. 1–11, Nov. 2020, doi: 10.3390/met10111425.

24. Sharma and V. K. Dwivedi, “Influence of tool rotational speed on mechanical properties of aluminium alloy AA 7075-T6 during friction stir welding process,” Advances in Materials and Processing Technologies, vol. 8, no. sup2, pp. 886–898, 2022, doi: 10.1080/2374068X.2021.1953928.

25. J. Iwaszko and M. Sajed, “Technological aspects of producing surface composites by friction stir processing—a review,” Journal of Composites Science, vol. 5, no. 12, pp. 1–31, 2021, doi: 10.3390/jcs5120323.

26. I. Almazrouee, K. J. Al-Fadhalah, and S. N. Alhajeri, “A new approach to direct friction stir processing for fabricating surface composites,” Crystals (Basel), vol. 11, no. 6, Jun. 2021, doi: 10.3390/cryst11060638.

27. M. Khan, A. Rehman, T. Aziz, M. Shahzad, K. Naveed, and T. Subhani, “Effect of inter-cavity spacing in friction stir processed Al 5083 composites containing carbon nanotubes and boron carbide particles,” J Mater Process Technol, vol. 253, pp. 72–85, Mar. 2018, doi: 10.1016/j.jmatprotec.2017.11.002.

28. J. Iwaszko, K. Kudła, and K. Fila, “Technological aspects of friction stir processing of AlZn5.5MgCu aluminum alloy,” Bulletin of the Polish Academy of Sciences: Technical Sciences, vol. 66, no. 5, pp. 713–719, Oct. 2018, doi: 10.24425/125338.

29. M. Barmouz, V. Zall, and H. Pashazadeh, “Mechanical and microstructural characterization of hybrid Cu-SiC-Zn composites fabricated via friction stir processing,” Materials Research, vol. 19, no. 6, pp. 1292–1298, Nov. 2016, doi: 10.1590/1980-5373-MR-2016-0152.

30. M. Houshyar, S. Nourouzi, and H. Jamshidi Aval, “Sandwich Method: Strategy to Fabricate Al/SiC Composites by FSP,” Transactions of the Indian Institute of Metals, vol. 72, no. 12, pp. 3249–3259, Dec. 2019, doi: 10.1007/s12666-019-01793-y.

31. Y. Huang, T. Wang, W. Guo, L. Wan, and S. Lv, “Microstructure and surface mechanical property of AZ31 Mg/SiCp surface composite fabricated by Direct Friction Stir Processing,” Mater Des, vol. 59, pp. 274–278, 2014, doi: 10.1016/j.matdes.2014.02.067.

32. J. Iwaszko and M. Sajed, “Technological aspects of producing surface composites by friction stir processing—a review,” Journal of Composites Science, vol. 5, no. 12, pp. 1–31, 2021, doi: 10.3390/jcs5120323.

33. D. A. P. Prabhakar et al., “A comprehensive review of friction stir techniques in structural materials and alloys: challenges and trends,” Journal of Materials Research and Technology, vol. 20, pp. 3025–3060, 2022, doi: 10.1016/j.jmrt.2022.08.034.

34. R. S. Mishra, M. W. Mahoney, S. X. Mcfadden, N. A. Mara, and A. K. Mukherjee, “High strain rate superplasticity in a friction stir processed 7075 al alloy,” 2000. [Online]. Available: www.elsevier.com/locate/scriptamat.

35. R. Butola, L. Tyagi, R. M. Singari, Q. Murtaza, H. Kumar, and D. Nayak, “Mechanical and wear performance of Al/SiC surface composite prepared

through friction stir processing," Mater Res Express, vol. 8, no. 1, 2021, doi: 10.1088/2053-1591/abd89d.

36. Z. Ding, C. Zhang, L. Xie, L. C. Zhang, L. Wang, and W. Lu, "Effects of Friction Stir Processing on the Phase Transformation and Microstructure of TiO2-Compounded Ti-6Al-4V Alloy," Metall Mater Trans A Phys Metall Mater Sci, vol. 47, no. 12, pp. 5675–5679, 2016, doi: 10.1007/s11661-016-3809-8.

37. E. Toma Bane Karash, S. Rajab Yassen, and M. Taqi Elias Qasim, "The Effect of the Cutting Depth of the Tool Friction Stir Process on the Mechanical Properties and Microstructures of Aluminum Alloy 6061-T6," American Journal of Mechanics and Applications, vol. 3, no. 5, pp. 33–41, 2015, doi: 10.11648/j.ajma.20150305.11.

38. [38] H. I. Dawood, K. S. Mohammed, A. Rahmat, and M. B. Uday, "Effect of small tool pin profiles on microstructures and mechanical properties of 6061 aluminum alloy by friction stir welding," Transactions of Nonferrous Metals Society of China (English Edition), vol. 25, no. 9, pp. 2856–2865, Sep. 2015, doi: 10.1016/S1003-6326(15)63911-5.

39. Jebur, S. Amin, and I. Mahmood, "The Influence of Ultrasonic Impact Peening on the Mechanical Properties of Similar Friction Stir Welded Joints of AA 7075-T73," Engineering and Technology Journal, vol. 39, no. 9, pp. 1345–1351, Sep. 2021, doi: 10.30684/etj.v39i9.1725.

40. D. S. C. Mouli, K. A.Sarath, and R. R. U. Maheswara, "Improvement of Hardness of Aluminium 7075 Metal Matrix Composite with Silicon Carbide Powder by Friction Stir Processing," International Journal of Engineering Technology Science and Research, vol. 4, no. 9, pp. 432–439, 2017.

41. K. Li, X. Liu, and Y. Zhao, "Research status and prospect of friction stir processing technology," Coatings, vol. 9, no. 2. MDPI AG, 2019. doi: 10.3390/COATINGS9020129.

42. K. G. Watkins, M. A. Mcmahon, and W. M. Steen, "Microstructure and corrosion properties of laser surface processed aluminium alloys: a review," 1997.

43. P. Parandoush and A. Hossain, "A review of modeling and simulation of laser beam machining," International Journal of Machine Tools and Manufacture, vol. 85. Elsevier Ltd, pp. 135–145, 2014. doi: 10.1016/j.ijmachtools.2014.05.008.

44. C. S. Wu, L. Wang, W. J. Ren, and X. Y. Zhang, "Plasma arc welding: Process, sensing, control and modeling," J Manuf Process, vol. 16, no. 1, pp. 74–85, Jan. 2014, doi: 10.1016/j.jmapro.2013.06.004.

45. C. Nouguier-Lehon, M. Zarwel, C. Diviani, D. Hertz, H. Zahouani, and T. Hoc, “Surface impact analysis in shot peening process,” Wear, vol. 302, no. 1–2, pp. 1058–1063, Apr. 2013, doi: 10.1016/j.wear.2012.11.031.

46. B. Bhattacharyya, S. Mitra, and A. K. Boro, “Electrochemical machining: new possibilities for micromachining,” 2002.

47. [47] K. H. Ho and S. T. Newman, “State of the art electrical discharge machining (EDM),” Int J Mach Tools Manuf, vol. 43, no. 13, pp. 1287–1300, 2003, doi: 10.1016/S0890-6955(03)00162-7.

48. T. B. Thoe, D. K. Aspinwall, and M. L. H. Wise, “Review on ultrasonic machining,” 1998.

49. M. Akbari, P. Asadi, and T. Sadowski, “A Review on Friction Stir Welding: Numerical Modeling,” 2023, doi: 10.20944/preprints 202307.1296.v1.

50. Z. Y. Ma, B. L. Xiao, and D. Wang, “Challenge and opportunities for friction stir welding of discontinuously reinforced metal matrix composites.”

51. Y. X. Gan, D. Solomon, and M. Reinbolt, “Friction stir processing of particle reinforced composite materials,” Materials, vol. 3, no. 1, pp. 329–350, 2010, doi: 10.3390/ma3010329.

52. R. Bauri and D. Yadav, Metal matrix composites by friction stir processing. Elsevier, 2017. doi: 10.1016/C2016-0-04019-6.

53. V. Kumar, S. Angra, and S. Singh, “Influence of rare earth elements on aluminium metal matrix composites: A review,” Materials Physics and Mechanics, vol. 51, no. 2, pp. 1–20, 2023, doi: 10.18149/MPM.5122023_1.

54. T. C. Joshi, S. S. Rathore, V. V. Dabhade, and U. Prakash, “Dry sliding wear behavior of sinter forged micrometric and nanometric yttrium oxide reinforced AA-7075 matrix composites,” Journal of Alloys and Metallurgical Systems, vol. 6, no. March, p. 100067, 2024, doi: 10.1016/j.jalmes.2024.100067.

55. G. Lin et al., “Influence of cerium and yttrium addition on strength and electrical conductivity of pure aluminum alloys,” Journal of Rare Earths, vol. 42, no. 3, pp. 600–611, 2024, doi: 10.1016/j.jre.2023.09.019.

56. K. Choudhary and R. Jain, “Fundamentals of Friction Stir Welding, Its Application, and Advancements,” 2021, pp. 41–90. doi: 10.1007/978-3-030-63986-0_2.

57. “Standard Test Methods for Tension Testing of Metallic Materials ASTM-E8-E8M-09”.

58. “E3 Standard Practice for Preparation of Metallographic specimens”.

59. “Designation: E407 − 07′107′1 Standard Practice for Microetching Metals and Alloys 1”, doi: 10.1520/E0407-07.

60. “Metallic materials-Vickers hardness test-Part 1: Test method Matériaux métalliques-Essai de dureté Vickers-INTERNATIONAL STANDARD ISO 6507-1,” 2023. [Online]. Available: www.iso.org

61. “Standard Test Method for Wear Testing with a Pin-on-Disk Apparatus 1 Characteristics of the Interlaboratory Wear Test Specimens”, doi: 10.1520/G0099.

62. “Standard Test Methods for Bend Testing of Material for Ductility 1”, doi: 10.1520/E0290-1.

63. X. Feng, H. Liu, and J. C. Lippold, “Microstructure characterization of the stir zone of submerged friction stir processed aluminum alloy 2219,” Mater Charact, vol. 82, pp. 97–102, 2013, doi: 10.1016/j.matchar.2013.05.010.

64. L. Ingemarsson and M. Halvarsson, “SEM/EDX ANALYSIS OF BORON A case study”.

65. S. Rohani Mojarad, “Friction Stir Welding of Al 2024 with Al 7075 Alloys and evaluate its structural and mechanical properties ARTICLE INFO ABSTRACT,” Journal of Advanced Materials and Processing, vol. 6, no. 4, pp. 53–64, 2018.

66. E. J. Pavlina and C. J. Van Tyne, “Correlation of Yield strength and Tensile strength with hardness for steels,” J Mater Eng Perform, vol. 17, no. 6, pp. 888–893, 2008, doi: 10.1007/s11665-008-9225-5.

67. M. Hanief and M. S. Charoo, “Archard’s wear law revisited to measure accurate wear coefficient considering actual sliding velocity,” in Materials Today: Proceedings, Elsevier Ltd, 2021, pp. 5598–5600. doi: 10.1016/j.matpr.2021.03.475.

68. R. Chitwadgi, B. Siddesh, B. L. Shankar, R. Suresh, and N. G. Siddeshkumar, “Optimization and analysis of dry sliding wear behaviour of n-b4c/mos2 ureinforced aa2219 nano hybrid composites using response surface methodology,” Metallurgical and Materials Engineering, vol. 28, no. 3, pp. 469–485, Sep. 2022, doi: 10.30544/840.

RESUME

Ahmed Abdullah Khalaf KHALAF graduated first and elementary education in Iraq. He completed high school education in Government Boys Higher Secondary School Baghdad City, after that, he started undergraduate program in University of Technology - Baghdad - Department of Materials Engineering in 2003, and he finished his bachelor's degree in 2007. He came to Turkey in 2021 for master's degree in metallurgical and materials engineering in Karabuk University.